AFCRL-67-0013

LIDAR-RADAR LOWER ATMOSPHERIC OBSERVATIONS

By

WILLIAM VIEZEE JOHN OBLANAS

CONTRACT AF 19(628)-5976
PROJECT NO. 6670
TASK NO. 667007

Final Report

Period Covered: 1 April 1966 thru 11 November 1966

Date of Report: 14 December 1966

Contract Monitor: WILBUR H. PAULSEN

Prepared for

AIR FORCE CAMBRIDGE RESEARCH LABORATORIES
OFFICE OF AEROSPACE RESEARCH
UNITED STATES AIR FORCE
BEDFORD, MASSACHUSETTS 01730

STANFORD RESEARCH INSTITUTE

MENLO PARK, CALIFORNIA

STANFORD RESEARCH INSTITUTE
MENLO PARK CALIFORNIA

AFCRL-67-0013

LIDAR-RADAR LOWER ATMOSPHERIC OBSERVATIONS

By

WILLIAM VIEZEE JOHN OBLANAS

SRI Project 5982

CONTRACT AF 19(628)-5976
PROJECT NO. 6670
TASK NO. 667007

Final Report

Period Covered: 1 April 1966 thru 14 November 1966

Date of Report: 14 December 1966

Contract Monitor: WILBUR H. PAULSEN

Prepared for

AIR FORCE CAMBRIDGE RESEARCH LABORATORIES
OFFICE OF AEROSPACE RESEARCH
UNITED STATES AIR FORCE
BEDFORD, MASSACHUSETTS 01730

Copy No. 1

ABSTRACT

Simultaneous observations of the lower atmosphere with lidar (laser radar) and microwave radar are summarized. The observations are restricted in space to the location of Stanford Research Institute, Menlo Park, California, and in time to June, August, and September 1966. Lidar echoes from the clear lower atmosphere are compared with the temperature and humidity data from the rawinsonde ascents made at Oakland, California.

During clear skies, no radar or lidar echoes were observed above 2000 m. Below this level the atmospheric structure that was analyzed from the lidar data showed a diurnal variation similar to that of the thermal stability of the atmosphere. Other time-dependent variations that were evident in the data are believed to be related to short period changes in the height of the top of the marine layer. No specific relationship was found between the lidar data and the rawinsonde data from Oakland.

Radar echoes observed in the clear lower atmosphere were classified as meteorological angels.

CONTENTS

CONTENTS (Continued)

ILLUSTRATIONS

TABLES

PROJECT ORGANIZATION AND ACKNOWLEDGEMENT

This project was carried out under the direct supervision of Mr. R. T. H. Collis by Messrs. Viezee and Oblanas, the authors of this report. The authors wish to acknowledge Mr. Collis' assistance at all stages of this project and, in addition, wish to thank Mr. Fred Fernald for his help in the scheduling of observations and Dr. Paul Davis for his various suggestions as to the interpretation of the data.

I INTRODUCTION AND SUMMARY

This report summarizes observations of the lower atmosphere made with calibrated optical (laser) radars at wavelengths of 0.6943μ and 1.06μ and a calibrated K_a-band microwave radar at a wavelength of 8.6 mm. The purpose of the observations was to determine:

(1) The utility of optical radar for the detection and measurement of such meteorological phenomena of the lower atmosphere as temperature inversions, heights and thickness of haze layers, and humidity variations.

(2) The nature of observations that can be made with lidar but cannot be made with high-performance K_a-band radar such as the AN/TPQ-11.

(3) The optimum characteristics of an optical instrument suitable for routine operational use in indirect measurement of temperature, humidity, or wind as a function of height.

All observations were made at the location of Stanford Research Institute at Menlo Park, California, during June, August, and September 1966. The meteorological conditions encountered were those characteristic of the California coastal regions during the summer, i.e., a high frequency of occurrence of low-level temperature inversions below which haze, fog, smog or stratus were present in variable amounts. These atmospheric conditions are in accordance with the purpose for which the observations were made. Supporting meteorological data were derived from standard rawinsonde ascents made twice daily at nearby Oakland.

Three optical radars (lidars) were used in the observation program, the Mark I and Mark II ruby lidars (0.6943μ), and the Mark V neodymium lidar (1.06μ). The Mark I and Mark V lidars were operated with varying elevation angles; the Mark II lidar and the K_a-band radar were operated pointing vertically upward. Pertinent information on equipment and on the format in which the radar and lidar data were obtained is given in Section II.

Data for three separate time periods are presented in Section III. During each period, a particular aspect of the equipment and data was investigated. During the first period (13 June through 23 June 1966) the collection and display of data during simultaneous operation of the radar and lidars were tested. Also, the initial response of the radar and ruby lidar to clear sky conditions was evaluated. During the second period (16 August through 26 August 1966) detailed observations with the ruby lidar were made twice daily during clear sky conditions. These observations were compared with the temperature and humidity data from the rawinsonde ascents made at Oakland. During the third period (14 September through 15 September 1966) observations of the clear lower atmosphere were made with the radar and the ruby and neodymium lidars for periods of up to 12 hours in order to investigate time-dependent variations in the atmospheric structure as analyzed from the data.

Under clear sky conditions, no lidar echoes were apparent above 2000 m. However, below this level, a detailed structure of the lower atmosphere could be analyzed from the lidar data showing time-dependent variations. Some of these variations were obviously related to the daily march of the thermal stability of the atmosphere, while others appeared related to variations in the height of the upper boundary of the low-level marine layer. From visual observations it was evident that changes in the distribution and concentration of haze and smog were reflected in the lidar data. However, identification of the lidar echoes in terms of specific physical structure or composition of the atmosphere could not be made with the data from the Oakland rawinsonde ascents, possibly because of differences in scale between lidar and rawinsonde data and differences in the geographical location between SRI and Oakland (about 20 miles). It is suggested that a probe be used to provide the vertical structure of temperature, humidity, and aerosol content at the same location where the lidars are operated and on a scale similar to that given by the lidar data. An instrument package attached to a tethered balloon seems most desirable.

The radar echoes received from a visually clear atmosphere were classified as meteorological angels. They occurred invariably below 1500 m. At times they were related to the surface temperature. Their exact origin is discussed in existing literature on meteorological radar angels [Atlas, 1959, 1960].

When visually dense clouds were viewed, the microwave radar gave superior information on cloud structure and cloud thickness, but tenuous clouds could be located with the ruby lidar only.

The optimum characteristics of a lidar suitable for probing the lower atmosphere are described in Section IV. The characteristics are those visualized at the present time on the basis of the experience accumulated during the various phases of the observation program. The operation of the lidar at varying elevation angles seems essential.

II INSTRUMENTATION AND DATA RECORDING

A. SENSORS

The instrumentation used in this program consisted of the Stanford Research Institute Mark I and Mark II ruby lidars, the Mark V neodymium lidar, and the AN/AMQ-15 radar, along with the necessary data recording equipment. Figure 1 illustrates where the various instruments were located at the time the observations were made. The observation site, as shown in the figure, is photographed from a 35-foot-high observation tower.

1. Radar

The AN/AMQ-15 radar, originally designed for airborne use to measure cloud base and top height, was manufactured by Bendix Aviation in 1959. This equipment was subsequently converted by SRI into a ground-based, vertically pointing cloud radar. The operating characteristics of the AMQ-15 are quite similar to those of the AN/TPQ-11 radar. The principal differences are that the TPQ-11 has a larger receiving aperture and a narrower beamwidth, it utilizes separate transmitting and receiving antennas, and it has provision for a facsimile recorder. Neither equipment employs pulse-to-pulse signal integration as a method of improving system performance.

The parameters of these two radar systems are compared in Table I. All of the AMQ-15 parameters listed have been measured at SRI during the course of this program. The TPQ-11 data were obtained from Air Weather Service [1961], Katzenstein and Marson [1961], and Petrocchi and Paulsen [1966]. The following parameters of the two radars are significant in comparing overall detection sensitivity: peak power, pulsewidth, receiver aperture, and minimum discernable signal. Since the minimum discernable signal achieved by the TPQ-11 under operating conditions is unavailable, a calculated value of -99.0 dBm was used. A comparison of the above

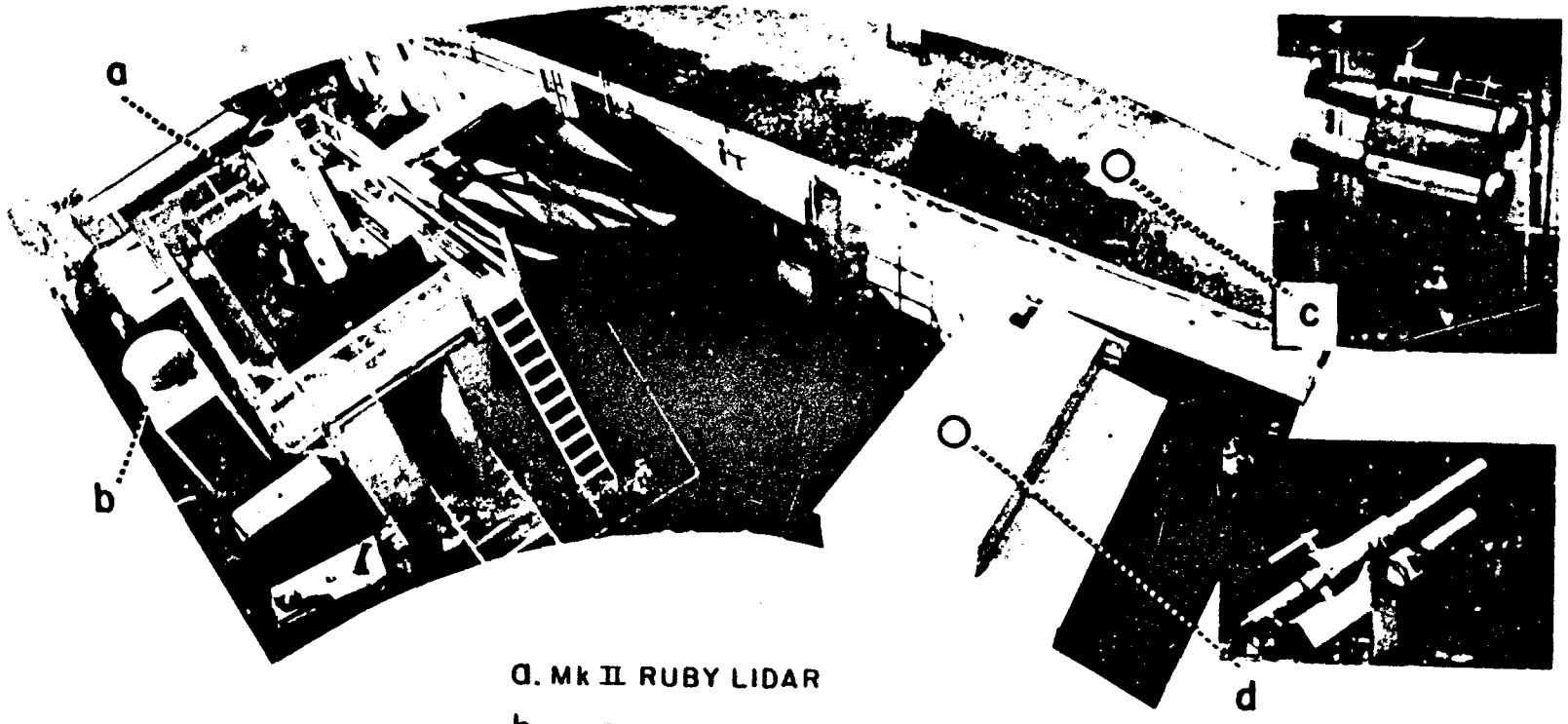

a. Mk II RUBY LIDAR

b. K_a- BAND MICROWAVE RADAR

c. Mk IV NEODYMIUM LIDAR

d. Mk I RUBY LIDAR

FIG. 1 EQUIPMENT LOCATION AT OBSERVATION SITE

Table I

RADAR EQUIPMENT PARAMETERS

	AN/AMQ-15	AN/TPQ-11
Transmitter		
Peak Power (kW)	20	100
Frequency (GHz)	34.9 (λ = 8.6 mm)	35
Pulse Width (μs)	0.8	0.5
PRF (pps)	667	1000
Antenna		
Diameter (m)	1.22	2.13
3-dB Beamwidth (deg)	0.5	0.25
Gain (dB)	49	53
First Sidelobe Level (dB)	-24	--
Receiver		
IF Frequency (GHz)	30	60
3-dB Bandwidth (GHz)	2.0	2.0
Overall Noise Figure (dB)	13	12
Dynamic Range (dB)	80 {10-dB linear; 70-dB logarithmic	0-15 dB linear mode; 5-65 dB logarithmic mode
Minimum Discernible Signal (dBm)	-96	-99 (calculated)
Minimum Range (m)	458	458
Range Resolution (m)	120	152
Performance Monitor	AN/UPM-14	AN/UPM-14

factors shows that the TPQ-11 has a 10.4-dB advantage in detection sensitivity, which corresponds to a 3.3:1 range advantage for targets of equal backscatter cross section.*

2. Lidar

Both the basic concepts of lidar detection of meteorological targets and the lidar equipment design features have been well documented in the open literature [Ligda, 1965; Collis, 1966; Northend, Honey, and Evans, 1966] and will not be repeated here.

The significant parameters of the Mark I, Mark II, and Mark V lidars used on this program are listed in Table II. All three lidars are quite similar in basic design, the major differences being refinements in the optical characteristics and engineering details necessary to optimize the lidars for specific types of observation programs. The specific refinements will be discussed in more detail in Section IV.

B. RELATIVE ROLES OF LIDAR AND RADAR AS ATMOSPHERIC PROBES

It is important to recognize the way in which lidar and K_a-band radar function as meteorological probes and to examine how they differ.

Both seek to establish the reflectivity (or backscatter) of the atmosphere to electromagnetic energy remotely as a function of range. This evaluation is complicated where substantial attenuation occurs--a condition which in both cases normally accompanies high reflectivity. Reflectivity of electromagnetic energy at a given wavelength depends primarily on the size, nature, and number of the particles constituting the atmospheric target. Because of the approximate 4-orders-of-magnitude decrease in transmitted wavelength (0.6943μ vs 8 mm), the lidar can detect particulate matter in suspension in the atmosphere of sizes and in concentrations small enough to be invisible to the eye. Reflections from the visually clear atmosphere are thus obtained, in addition to reflections from visible cloud, fog, or haze. In the case of millimetric radar,

* Assuming an R^{-2} propagation law for beam-filling volume targets; also, atmospheric attenuation considered negligible.

Table II

LIDAR EQUIPMENT PARAMETERS

	Mark I	Mark II	Mark V
Transmitter			
Laser Material	Ruby	Ruby	Neodymium-doped glass
Wavelength (Å)	6943	6943	10,600
Peak Power Output (W)	10^7	10^7	2×10^7
Pulse Width (ns)	30	35	22
Optics	4" dia. refractor	12.5" dia. reflector	6" dia. reflector
Beamwidth (mrad)	0.87	0.3	0.5
Firing Rate (ppm)	1	1	4
Q-Switch	saturable dye cell	rotating prism	rotating prism
Receiver			
Optics	4" refractor	12.5" reflector	6" reflector
Field of View	← variable →		
Predetection Filter Wavelength Interval (Å)	17	12.4	98.5
Detector	RCA 7265 Photomultiplier (S-20 response)	ITT FW-130 Photomultiplier (S-20 response)	RCA 7102 Photomultiplier (S-1 response)
Post-detection Filter Bandwidth (GHz)	6	30	6
Type of Receiver	Logarithmic	Linear	Logarithmic

returns may only be expected when particles of appreciable size are present in sufficient numbers per unit volume. In practice with radars having performance comparable to the TPQ-11, returns will be obtained from natural clouds only. In addition to the detection of energy by particulate scattering, it is possible that sufficient energy can be backscattered by dielectric inhomogeneities (in the gaseous atmosphere) at radar wavelengths to give rise to detectable echoes.

Assuming that it is possible to determine atmospheric reflectivity by both radar and lidar, the all-important question is: "What is the significance of this reflectivity or its changes in space and time in terms of meteorological factors?" At the wavelengths of storm-detecting weather radars (3 cm and longer) a fairly consistent relationship has been established between radar reflectivity and precipitation rate. At millimetric wavelengths, although attempts have been made to establish similar relationships between reflectivity and meaningful meteorological parameters, such as the water content of clouds, results have only limited application. For the most part, K_a-band radar observations are qualitative and are of most value in representing the envelope of detectable cloud and precipitation and their relative density. With lidar observations, similar qualitative deductions can be made, but in addition it has been found possible to evaluate the turbidity of "clear air" or air of limited transparency.

The difference in what is observed in the atmosphere by lidar and K_a-band radar, and what may be inferred in terms of meteorological significance from such observations is the subject of this study.

In addition to the shorter output wavelength of the lidar, the unique characteristics of laser radiation produce the following basic differences between the lidar and TPQ-11 radar:

(1) A higher resolution produced by an approximately 30:1 decrease in transmitter beamwidth (0.3 mrad vs 0.5 deg)

(2) A higher range resolution produced by an approximately 16:1 decrease in transmitting pulsewidth (30 ns vs 0.5 μs)

(3) An increase in system sensitivity produced by an approximate 2-order-of-magnitude increase in transmitter power output (10^7 Watts vs 10^5 Watts).

A further important difference results from the signal detection techniques used in lidar and radar systems. Each particle of an extended assemblage of scatterers comprising a lidar or radar target has a random phase position and may also be in motion. The instantaneous return from a volume of scatterers contributing simultaneously to a signal is thus a function of the net vector sum of the returns from each particle in the volume.

Since the relative positions of the scatterers are constantly changing, the net vector sum will vary from one pulse to the next, and a meaningful assessment of signal intensity can only be achieved by averaging [Marshall and Hitchfeld, 1953]. The averaging of statistically independent signals may be accomplished by at least two methods:

(1) Averaging the return signals produced by a series of successive transmitted pulses

(2) Averaging the return signals from a single transmitted pulse collected by several antennas that are located near the radar transmitter.

In the case of radar, method (1) is the most frequently employed averaging process. In the case of the lidar, method (2) is employed as follows: The lidar uses imaging optics and a detector that makes independent measurements of received power at many points on its surface [Helstrom, 1964]. Thus, the detector surface acts as a large array of receivers, each of which produces a number of photoelectrons proportional to received power. Since the measurements at the several hundred elements on the detector surface are independent, the total detector output can be considered their average. Therefore, the lidar receiver output is a measure of received power averaged over many individual measurements. A single lidar pulse, unlike a single radar pulse, thus provides an adequate basis for assessing lidar returns from distributed, atmospheric targets.

Method (2) above has been advantageous in terms of lidar development, because the lasers used for this application to date have only been capable

of producing pulses at intervals measured in seconds or tens of seconds, compared with the 1000 pps PRF of radars such as the TPQ-11. On the other hand, the slow data rate of such systems is very restrictive, in terms of probing extensive volumes of space by scanning or monitoring events with a short-time constant.

C. DATA RECORDING

The radar data were recorded in a conventional format similar to the facsimile recording used with the TPQ-11 radar. That is, a 35mm continuous-motion recording camera photographed an intensity modulated range sweep on the face of an oscilloscope. After processing, the film provided a height and signal intensity vs time history of the radar returns. A range sweep speed of 5 μs/cm corresponds to a total height scale on the film of zero to 7.5 km. A film speed of 41 mm/min. provided adequate time resolution.

Examples of this data format are illustrated in Figs. 2b and 3b, which show selected portions of the 35mm radar film record enlarged approximately 3 x. The bright horizontal band just above zero elevation is produced by transmitter main bang leakage into the receiver. The elliptical dot sometimes seen at the top of the figures represents time markers spaced one minute apart (See Fig. 3b).

The uniformly mottled appearance of the film is produced by the receiver noise level. Since threshold signals were of primary interest in this program, the intensity modulation and film exposure time were adjusted for faint recording of the receiver noise level, thus, any signal appearing above the noise level would also be recorded (see Fig. 9).

While the relative density of the negative film image is a good qualitative indication of relative signal intensity, this method does not lend itself to accurate determinations of signal amplitude. Accordingly, an A-scope (signal amplitude vs range) photograph of both the radar and lidar were taken at each lidar observation. These A-scope photographs, such as Figs. 2a and 3a, were the primary source of data for this study. All the radar A-scope photos in this report represent the return signal averaged over 66 radar pulses.

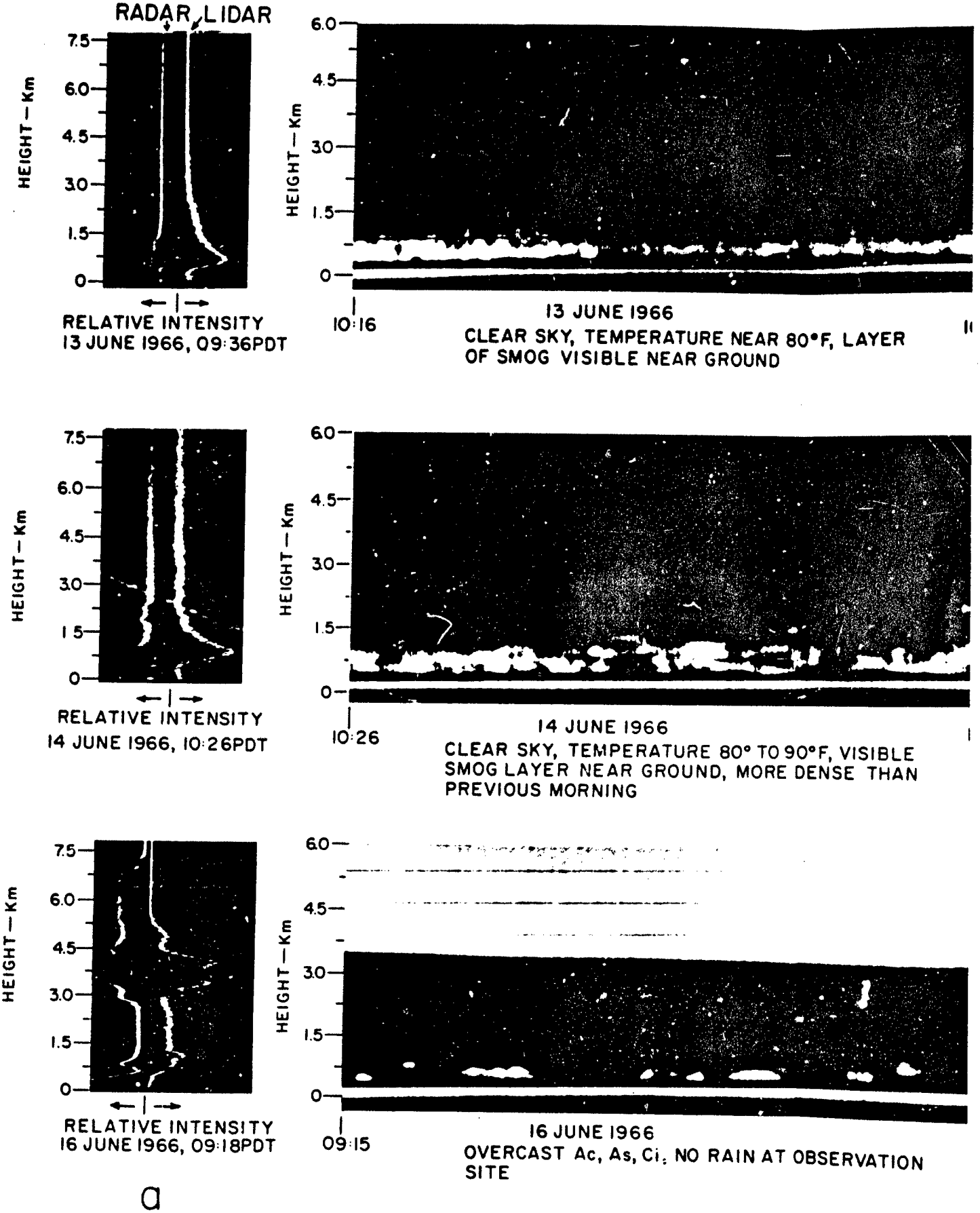

a

FIG. 2 DATA SAMPLES FROM
(a) Traces of Signal Inte

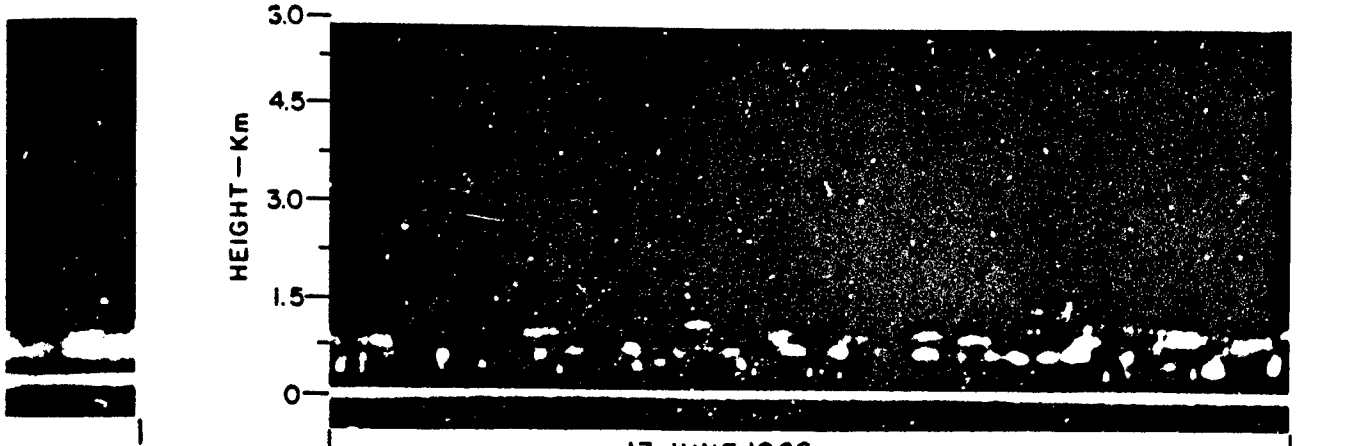

NO AFTERNOON DATA

E
N

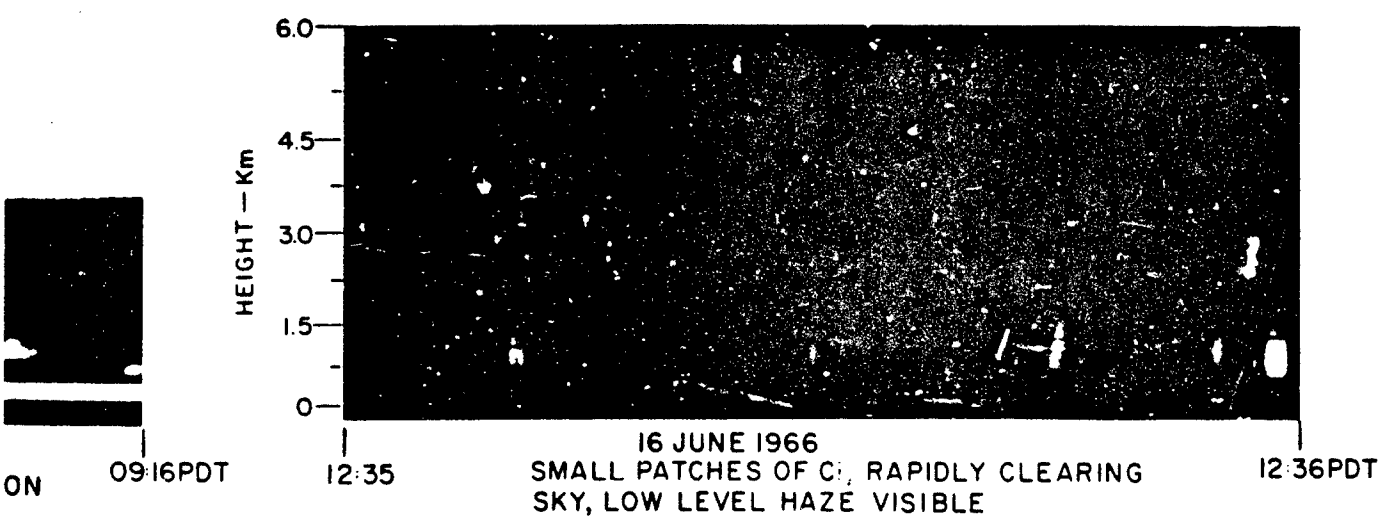

ON

b

› FROM RADAR AND LIDAR:
ınal Intensity Versus Height
ar Echoes for One Minute

B

FIG. 2

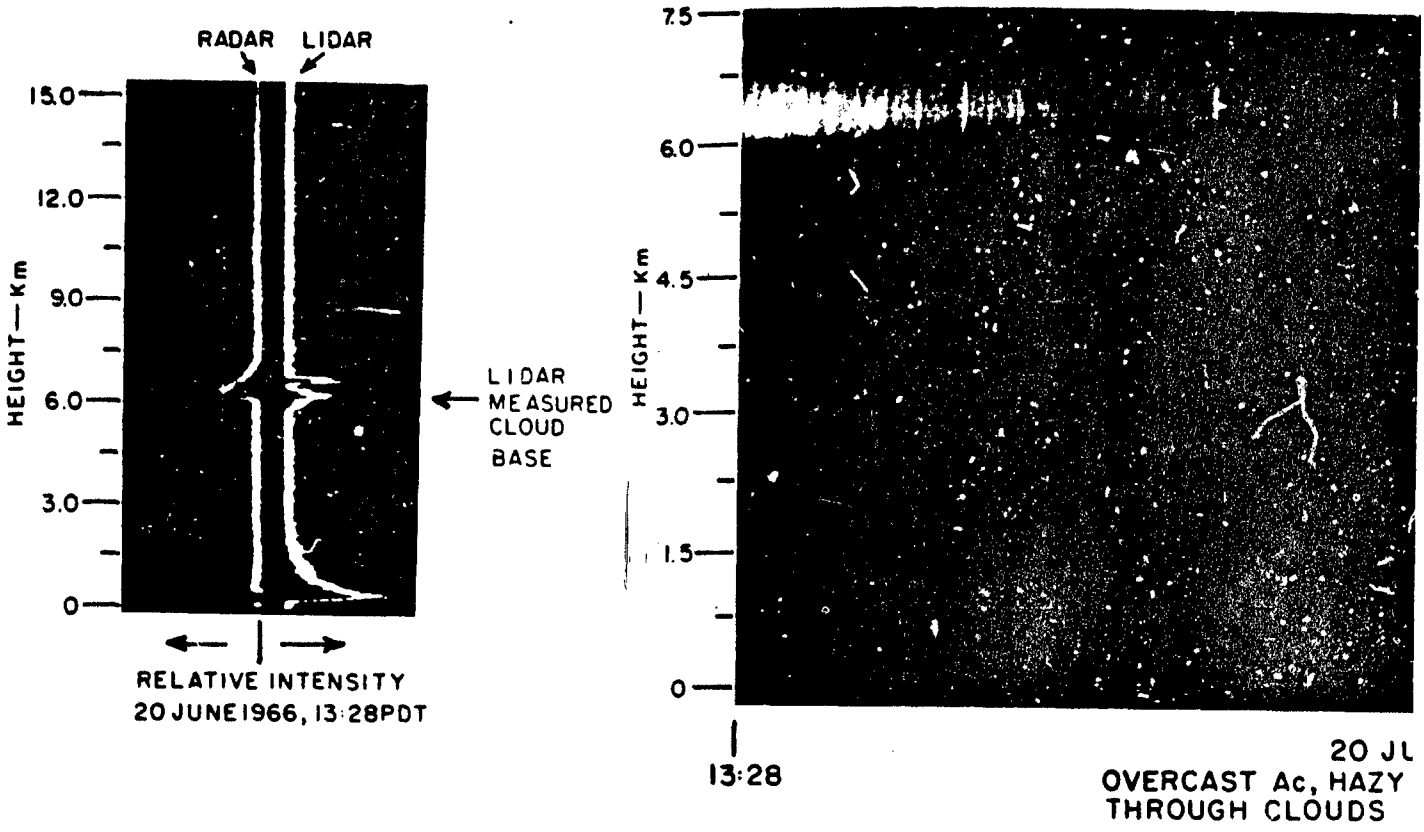

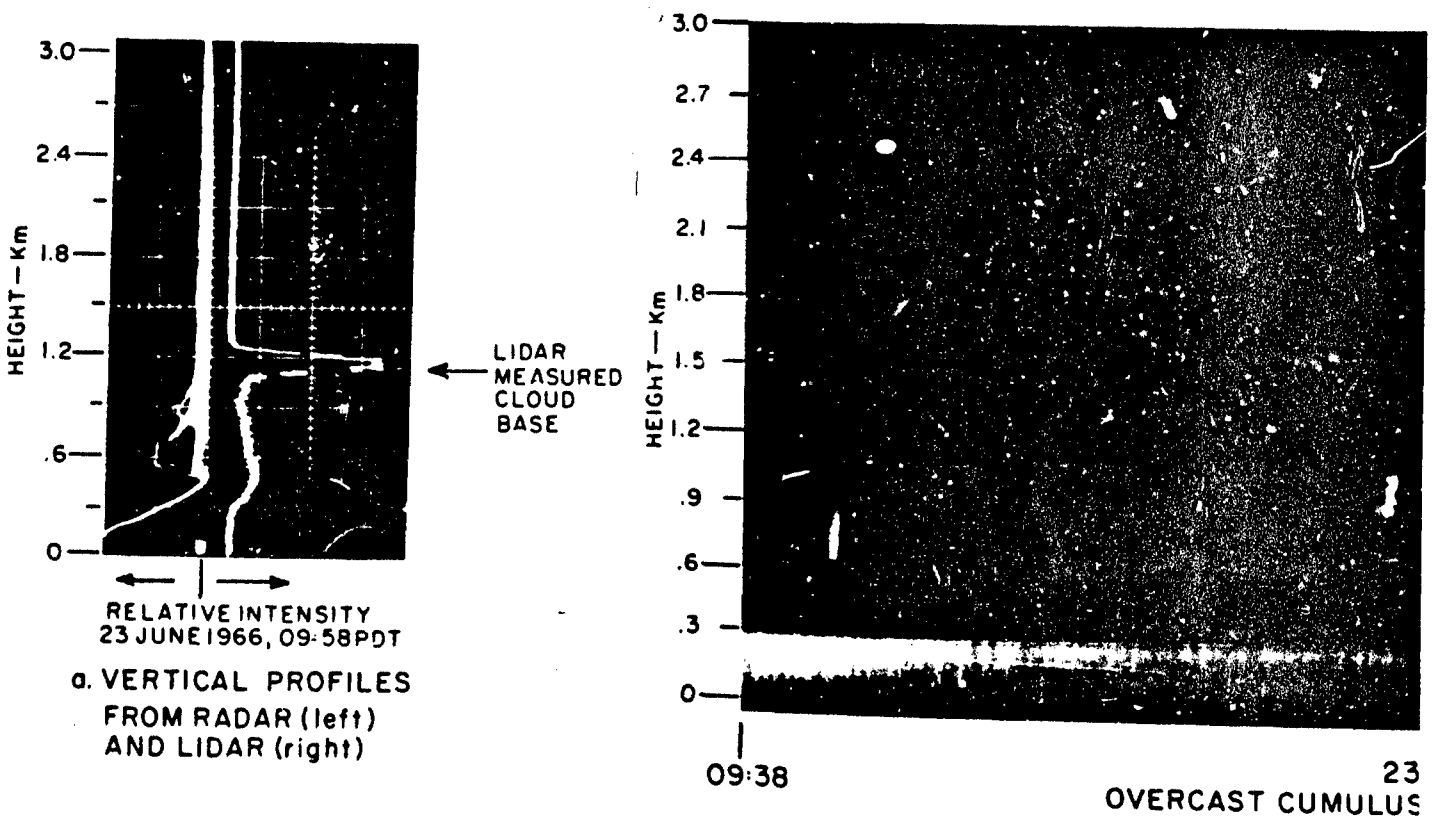

a. VERTICAL PROFILES FROM RADAR (left) AND LIDAR (right)

b. RADAR E(

FIG. 3 DATA SAMPLES FROM RADAR AND LI

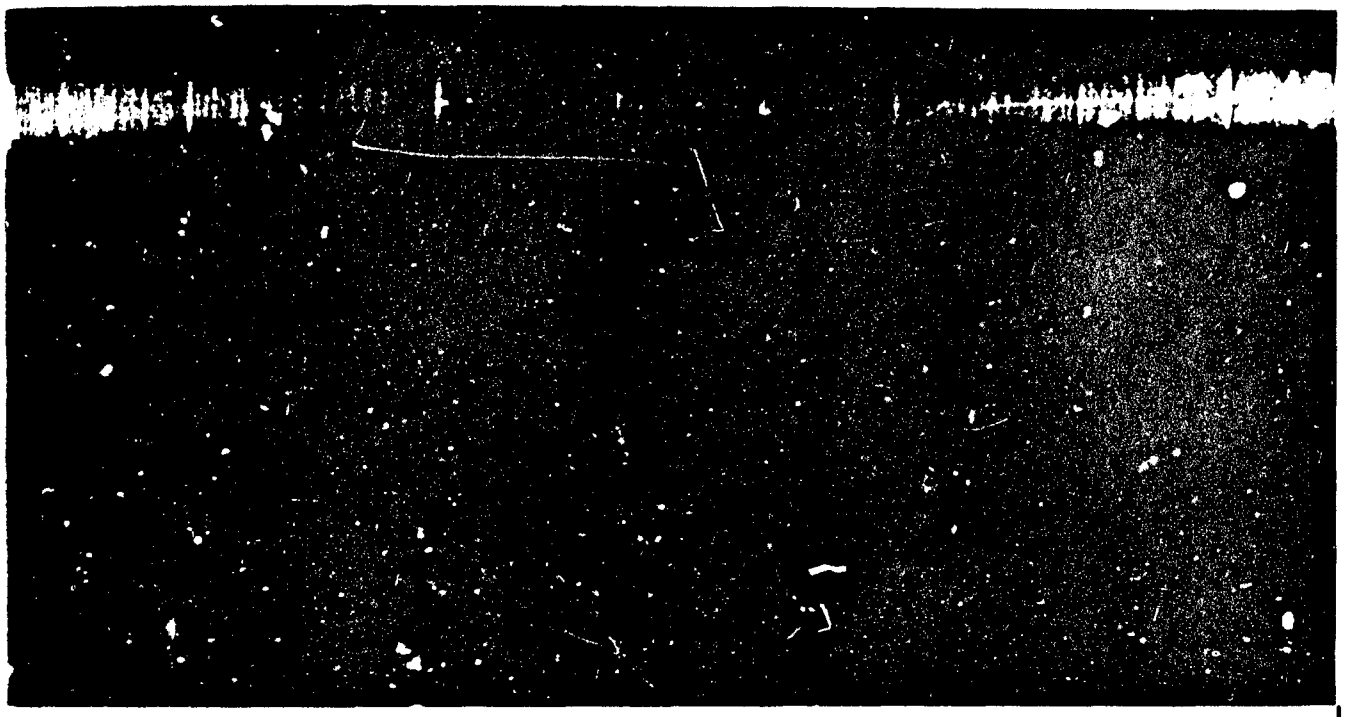

20 JUNE 1966
'8 OVERCAST Ac, HAZY SKY, SUN VISIBLE THROUGH CLOUDS 13:29PDT

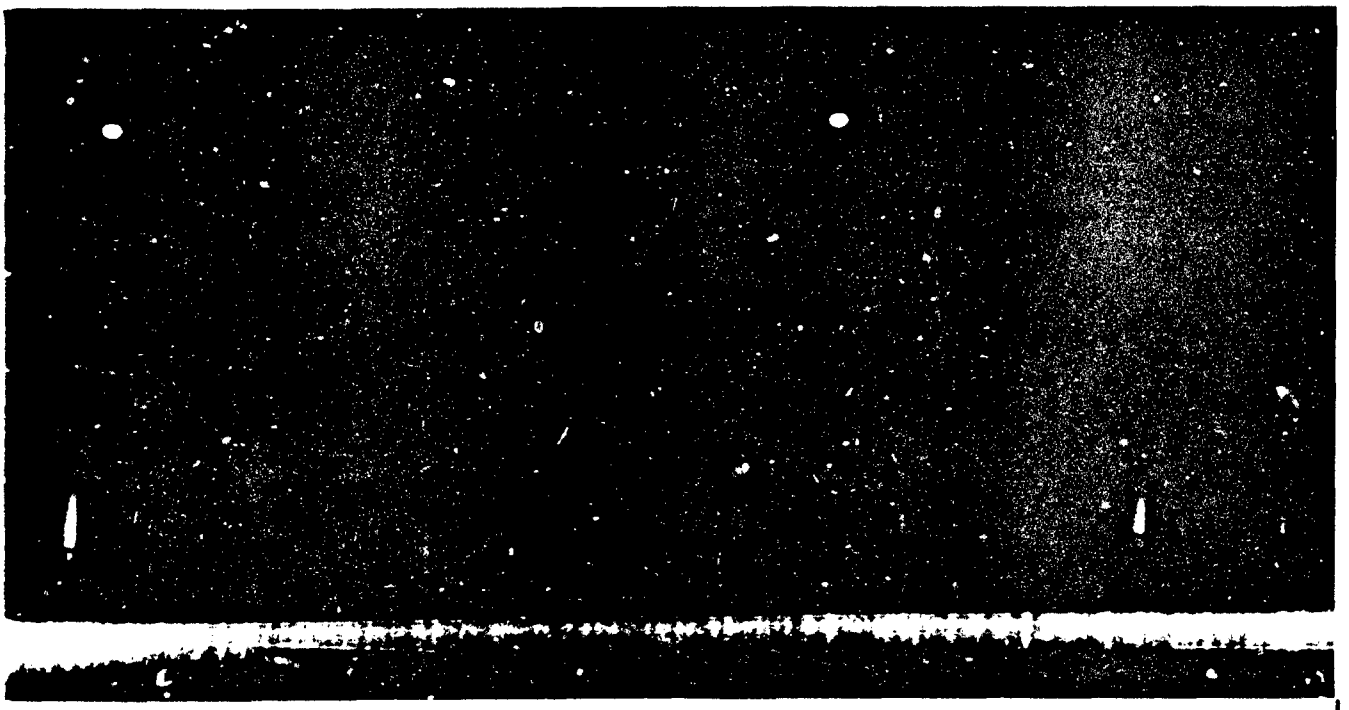

23 JUNE 1966
38 OVERCAST CUMULUS, DARK GREY IN APPEARANCE 09:40PDT

b. RADAR ECHOES

FIG. 3 DATA SAMPLES FROM RADAR AND LIDAR

FIG. 3

III OBSERVATION PROGRAM

A. OBSERVATIONS DURING THE PERIOD 13 JUNE THROUGH 23 JUNE 1966

1. General

Observations of the lower atmosphere with the K_a-band microwave radar and the Mark II ruby lidar began on 13 June 1966. For two hours in the morning and two hours in the afternoon the radar was to be operated continuously, while vertical "soundings" from the lidar were to be obtained every 3 minutes. Both the radar and lidar were pointed vertically upward.

As is often the case with observation programs, various difficulties arose during the first several days of operation. These difficulties prevented a continuous and consistent collection of data. For example, 13 June marked the beginning of a two-day "heat wave" during which temperatures in the local area exceeded 100°F. The high temperatures caused excessive heating of the ruby crystal in the lidar which, in turn, seriously affected the power output. Consequently, the initial lidar data became unreliable. After a CO_2-cooling unit had been installed, observations were continued. On 15 June, the transmitter-receiver alignment of the lidar became disturbed due to heating. Since attention was focussed primarily on echoes in the lower atmosphere, a correct alignment was essential. The realignment interrupted the lidar observation program.

On 16 June, thunderstorm activity ended the heat spell. Although considerable cloudiness was present from time to time, observations with both radar and lidar were continued until 24 June. At that time the observation program was re-evaluated on the basis of the experience gained with equipment and data.

The radar and lidar data collected in conjunction with the radiosonde ascents from nearby Oakland were mostly valuable in suggesting better usage of equipment and better observation techniques. For example, the temperature inversion layer that is a typical low-level feature of the radiosonde

ascent during the summer season had an upper boundary that was often below 1000 m and a lower boundary that was often near 200 m. Haze, smog, fog, or stratus were frequently present in the marine layer below the inversion. With the lidar pointing vertically upward, echoes below 600 m could not be reliably identified, because below this level the transmitter beam is only partially intercepted by the field of view of the receiver. The radar data showed echo patterns in the lower 1500 m of the atmosphere during both clear sky and cloudy sky conditions. These patterns changed in appearance from morning to afternoon and from day to day. While most of the radar echoes can possibly be classified as meteorological angels, it would be of interest to compare them with low-level lidar observations. Therefore, lidar observations were needed at elevation angles away from the vertical in order to move the low-level structure of the marine layer into the receiver field of view.*

The Mark I ruby lidar is a better instrument for close-in observations than the Mark II because it can easily be operated with a large range of elevation angles. Moreover, it is more dependable, owing to its basic design. Thus, it became evident that a switch from the Mark II to the Mark I ruby lidar would benefit the observation program.

The performance of the Mark II lidar and the K_a-band radar seemed optimum when observations were made of middle and high clouds.

2. Discussion of Data

Figures 2 and 3 show samples of radar and lidar data for periods during which observations were successful. Clear sky as well as cloudy sky data are presented. One or two minutes of cross section of the film on which radar echoes were recorded each day are shown in Figs. 2b and 3b. The selected sections are representative of the echo patterns that were

* When the transmitter beam and the field of view of the receiver converge at 600 m along slant range, the atmospheric structure at 200 m above the ground can be "seen" with lidar, using an elevation angle of about 19°.

prevalent. Samples of the traces of signal intensity versus height for radar and lidar are shown in Figs. 2a and 3a. These traces were recorded by simultaneous, instant photography of the radar and lidar scopes.

An interesting feature of Figures 2 and 3 is the variation in shape, intensity, and frequency of appearance of the radar echoes in the clear air below 1500 m. The echoes resemble those commonly referred to as meteorological angels. During the morning of 13 June (Fig. 2-b) they were continuous in time and slightly variable in intensity, but during the afternoon when surface temperatures rose above 100°F, they appeared like bubbles. Whether or not the echoes were actually related to buoyant bubbles of air could not be determined. It can be seen that the upper boundary of the layer in which the radar echoes occurred did not change from morning to afternoon, even though the low-level temperature inversion that was present in the morning ascent from Oakland was completely destroyed by the afternoon heating. Thus, in this case there is no evidence that the maximum height of the observed angel activity for the K_a-band radar increases with the surface temperature, as was shown for the 1.25 cm-radar by Planck [1956] and by Sal'man and Brylev [1965].

During the morning of 14 June (Fig. 2b) a weak radar echo, continuous in time, was recorded near 2000 m, above a layer in which numerous echoes of variable intensity originated. Unfortunately, the continuous echo could not be reproduced from the original film data, and therefore it is not clearly visible in Fig. 2b. However, the trace of signal intensity versus height for the radar (Fig. 2-a), clearly shows the echo near 2000 m. It seemed to originate from a reflecting boundary near the top of the temperature inversion. The vertical profile of signal intensity for the lidar suggests a change in atmospheric backscatter near the same level. Unfortunately, the data for this day were incomplete, and the possible origin of the radar and lidar echoes could not be determined.

On subsequent days, (16 June and 20 June), transient radar echoes remained below 1500 m, varying in shape, intensity and frequency of occurrence. On 23 June (Fig. 3b) discrete echoes occurred at a time when numerous cumulus clouds were observed. The low-level temperature inversion had deteriorated on this day. A close inspection of the radar

film showed discrete echoes up to 1500 m, even though the lidar-measured cloud base was near 1200 m (see the trace of signal intensity versus range in Fig. 3a). The radar responded only weakly to cumulus clouds that came into the field of view. The radar echoes observed in the clear air below the cumulus are most likely meteorological angels related to thermals. The existence of this type of radar angel is discussed by Atlas [1959].

The data of Figs. 2 and 3 served to illustrate the response of the K_a-band radar that could be expected from the clear lower atmosphere. Observed echoes resembled those commonly referred to as meteorological angels. They occurred invariably below 1500 m and showed no specific relation to the low-level temperature inversion of the Oakland radiosonde ascent. Their intensity suggested a maximum range of detection much larger than 1500 m, so that it is reasonably certain that no such echoes were present above 1500 m. The possible origin of meteorological radar angels is discussed by Atlas [1959, 1960].

Radar response to clouds that occurred during the observation period cannot be appreciated from the film strips shown in Figs. 2 and 3. The sensitivity of the radar scope was turned high in order to emphasize echoes from the clear atmosphere. Consequently, any response from clouds saturated the film. The ability of the microwave radar to map and identify clouds and cloud types is well documented [Wilk, 1958; Harper, 1966]. In this study, echoes from visible clouds were recorded whenever cloudiness happened to be present, for the purpose of ascertaining that both the radar and the lidar were operating properly. An evaluation of proper response can be made by comparing the traces of signal intensity versus range of the radar and lidar with visual observations of cloud density in the field of view. For visually dense clouds the lidar does not penetrate the cloud as much as the radar. On the other hand, for visually thin clouds the lidar often shows an echo, whereas the radar does not.

These two situations are illustrated by the vertical profiles of signal intensity in Fig. 4. The traces for 09:15 PDT (Fig. 4a) corresponded to a visually dense coverage of As, Ac, and Ci. Occasional light

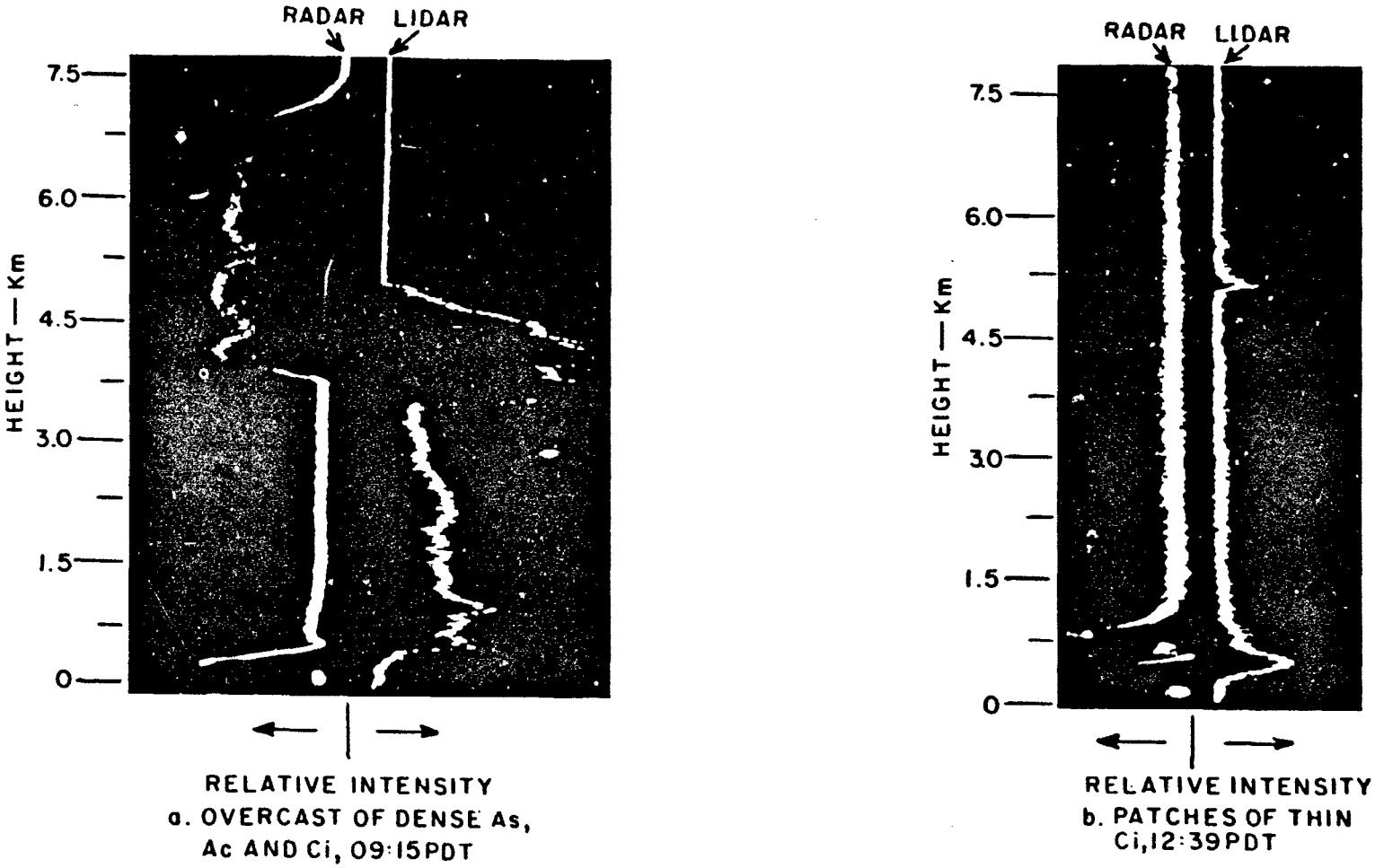

FIG. 4 TRACES OF SIGNAL INTENSITY VERSUS HEIGHT FROM RADAR AND LIDAR DURING CLOUDY SKY CONDITIONS, 16 JUNE 1966

rain was recorded in the area. It can be seen that the relative differences between the radar and lidar traces are in accordance with what would be expected on the basis of wavelength differences: the lidar shows significant response to the visually clear atmosphere below the cloud base (3500 m) but does not deeply penetrate the dense clouds, whereas the radar shows no return signal from below the clouds but penetrates deeply and possibly completely the dense cloud layer. The data for 12:39 PDT (Fig. 4b) show that the small patches of thin cirrus that came into the field of view were recorded by the lidar at a height of about 5 km but were not recorded by the radar, even though the gain setting of the radar oscilloscope was high. The large radar echo at 750 m was an angel. It is interesting to note that at the same level the lidar profile shows a marked increase in backscatter.

In order to demonstrate more quantitatively that the observed radar and lidar data were in accordance with theory, various traces of signal intensity versus height observed in clouds were compared with those computed on the basis of a simple cloud model. For this purpose the lidar/radar equation was written as follows:

$$P_r = P_t \frac{A_r}{R^2} \frac{1}{4\pi} \frac{C\tau}{2} \beta'_{180}(R') T_o T_a \exp\left[-2\int_o^{R'} \sigma \, dR'\right] \qquad (1)$$

where

P_r = received power (Watts)

P_t = transmitted power (Watts)

A_r = effective area of receiver aperture (m^2)

C = velocity of light (m/sec)

τ = transmitter pulse length (sec)

$\beta'_{180}(R')$ = volume backscattering coefficient at R' (m^{-1})

T_o = transmission efficiency of all optical components (dimensionless)

R = one-way distance to target (m)

R' = penetration distance into target (m)

T_a = atmospheric transmission factor accounting for total attenuation to and from the target (dimensionless)

σ = attenuation coefficient within target region (m^{-1})

Equation (1) can be written in the following form:

$$\frac{P_r}{P_t A_r \frac{1}{4\pi} \frac{C\tau}{2} T_o T_a} = \frac{1}{R^2}\beta'_{180}(R') \exp\left[-2\int_o^{R'} \sigma \, dR'\right] \qquad (2)$$

For convenience, the quantity $P_r/P_t A_r(1/4\pi)(C\tau/2)T_o T_a$ will be denoted by P in the following discussion.

Considering clouds only, the shape of the traces of signal intensity versus height for radar and lidar is basically determined by the variation of P with R. In Eq. (2), the quantity $P_t A_r T_o(C\tau/2)$ depends entirely on the equipment used, while T_a can be assumed constant for a given situation. Thus, P is linearly proportional to the intensity of the received signal. The volume backscattering coefficient, $\beta'_{180}(R')$, and the attenuation coefficient, σ, are properties of the target cloud. When a water cloud is vertically homogeneous, i.e., when β'_{180} and σ are constant with height or when β'_{180} and σ decrease with height, P is maximum near the cloud base and decreases rapidly thereafter due to range and cloud attenuation. Few of the amplitude traces that were observed during extensive cloudiness indicated a vertically homogeneous cloud or a cloud in which β'_{180} and σ decreased with height. However, the shape of the observed traces of signal intensity versus height were closely reproduced by assuming that β'_{180} had a simple relation to σ and, furthermore, that the liquid water content of the cloud increased linearly with height. With these assumptions, Eq. (2) can be written:

$$P \equiv \frac{P_r}{P_t A_r \frac{1}{4\pi} \frac{C\tau}{2} T_o T_a} = \frac{1}{R^2}(1 + \ell R')\beta'_{180} \exp\left[-\frac{\beta'_{180}}{k}(2 + \ell R')R'\right] \qquad (3)$$

where ℓ and k are constants that enter, respectively, into the assumed linear increase of liquid water content with height: $\beta'_{180}(R') = (1 + \ell R')\,\beta'_{180}$, and into an assumed linear relation of β'_{180} to σ : $\beta'_{180}(R') = k\,\sigma\,(R')$. In the above expressions, β'_{180} is the initial value of the volume backscattering coefficient at the base of the cloud. The assumption of a linear increase of liquid water content with height is reasonable in view of the relatively high cloud temperatures (0 to -10°C) indicated by the Oakland radiosonde ascent [Borovikov, et al., 1961].

Using Eq. (3), computations were made to reproduce the traces of signal intensity versus height observed for radar and lidar in visually dense As/Ac clouds during the morning of 16 June. Figure 5a shows the two selected sets of observed traces from radar and lidar, and Fig. 5b shows the corresponding computed traces of P versus height R, using $k = 1.5$ and $\ell = 1.5\ m^{-1}$. The value of k is in general agreement with that determined from the theory of Mie scattering; ℓ is arbitrary. In Fig. 5a, the ordinate is a linear height scale and the abscissa is a scale of relative units of receiver voltage. The relation between the strength of the returned signal and the receiver output is linear for the lidar but logarithmic for the radar. Therefore, computed values of P are presented on a log scale for the radar and on a linear scale for the lidar. Since the shape of the traces is of interest only, no absolute values are assigned to the abscissas. Values of P were computed from the base of the cloud (4000 m) up to 6500 m. For both sets of computations the initial values of the volume backscattering coefficient (β'_{180}) for radar and lidar that produced the shape of the computed traces are indicated in Fig. 5. In each case, the lidar is associated with a β'_{180} value that is larger than that for the radar by two orders of magnitude. The relative differences may be attributed to the associated differences in wavelength and to the relatively large absorption of microwave radiation by water spheres.

The good agreement between the traces of signal intensity versus height that are observed and those that are computed, between 4000 m and 6500 m, shows that the observations are compatible with theory.

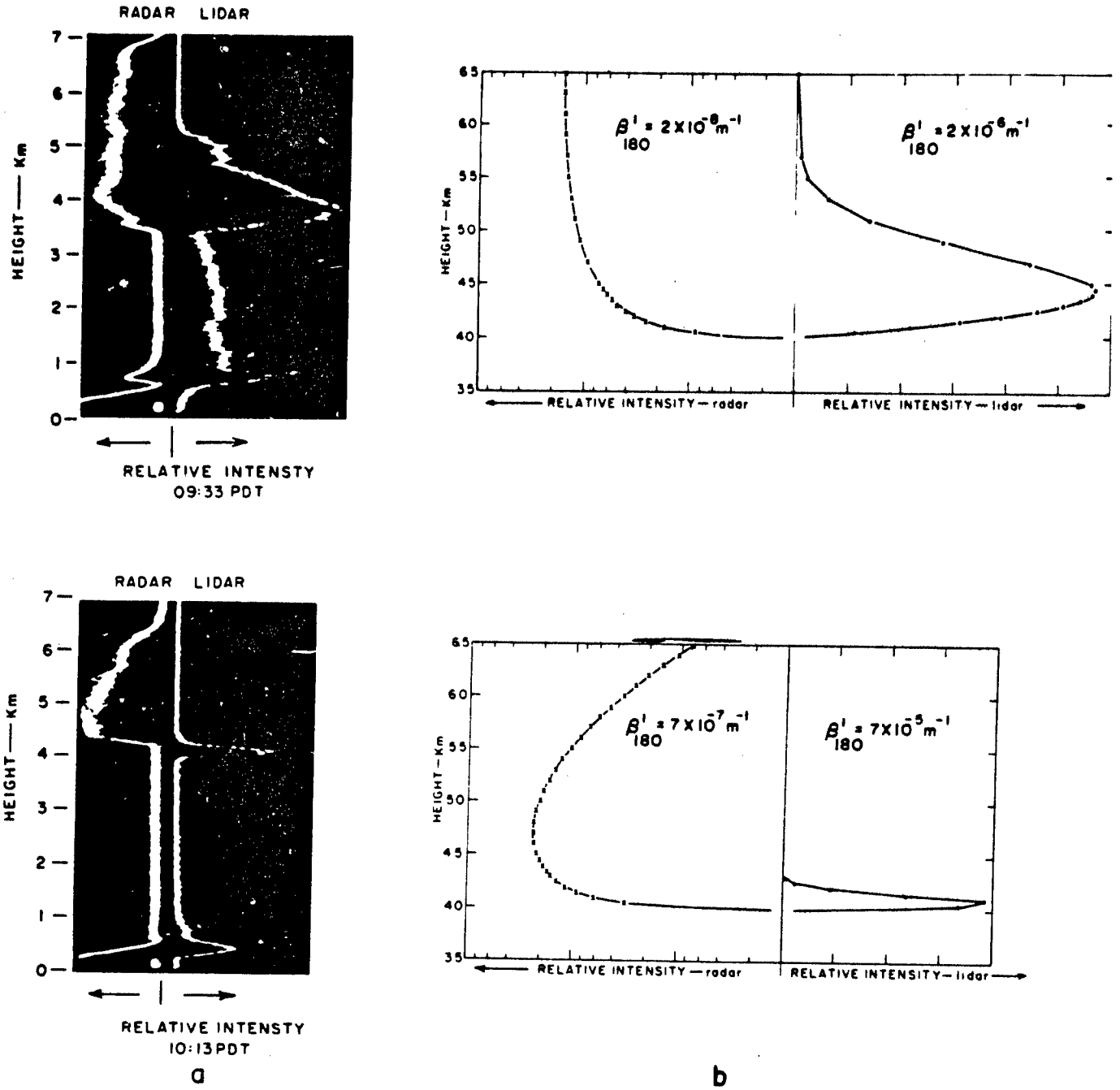

FIG. 5 OBSERVED (a) AND COMPUTED (b) TRACES OF SIGNAL INTENSITY VERSUS HEIGHT FOR RADAR AND LIDAR IN VISUALLY DENSE CLOUDS

Moreover, some qualitative information on cloud characteristics can be deduced from the changes in shape observed in the traces of signal intensity versus height from the radar and lidar. For example, in the case of the data shown in Fig. 5, the differences in the shape of the radar and lidar traces between 09:33 PDT (upper part of Fig. 5) and 10:13 PDT (lower part of Fig. 5) resulted from initial values of β'_{180} that differed by a factor of almost 10, which means that the liquid water content of the clouds was higher at 10:13 PDT.

B. OBSERVATIONS DURING THE PERIOD 16 AUGUST THROUGH 26 AUGUST 1966

1. General

Starting on 16 August 1966, a series of low-level observations were made with the Mark I ruby lidar, using elevation angles ranging from 3° to 75°. The purpose of the observations was to probe the structure of the lower atmosphere down to heights below 600 m during clear sky conditions. To make these observations, the Mark I lidar was equipped so that the output signal gave a presentation of the logarithm of the intensity of the signal returned from the atmosphere, versus range. The logarithmic output enables a recording of a wide range of signal strengths on a single display, and it facilitates data interpretation by displaying uniform exponentially decreasing signals as a straight line.

For each selected elevation angle, the trace of the logarithm of the signal intensity versus range that appeared on the lidar scope immediately after each single shot was recorded photographically. The atmospheric structure as analyzed from the lidar data was compared with the vertical profiles of temperature and humidity obtained from the radiosonde ascents at Oakland. Radar data were collected toward the end of the period.

2. Lidar Data

Figure 6 shows a typical sample of the lidar data and radiosonde data* that were collected during morning and afternoon. The sample of lidar data was obtained at elevation angles of 30° and 19.5°. These angles permit an analysis of atmospheric structure down to heights of 300 m and 200 m, respectively. The observations obtained during the morning (11:00 PDT) show a sharp decrease in atmospheric backscatter at a single level near 400 m. This decrease in backscatter marks the upper boundary of the local marine layer during the stable stratification of the lower atmosphere that prevails in the morning. High relative humidity and high amounts of haze and smog are characteristic features of the marine layer. The absence of a sharply defined boundary layer in the data for the afternoon (16:00 PDT) can be attributed to the effects of solar heating and the subsequent vertical mixing of the low-level aerosol due to convection. Comparing the lidar data and radiosonde data of Fig. 6, it is seen that the sharp decrease in backscatter observed near 400 m at 11:00 PDT does not correspond to any feature in the temperature and humidity profiles for Oakland obtained 6 hours earlier and later. However, the two changes in backscatter present in the afternoon data at heights of 300 m and 600 m correspond closely to the lower boundary (250 m) and the upper boundary (500 m) of the inversion layer in the temperature profile for 17:00 PDT.

Figure 7 illustrates the overall comparison between the location of the observed lidar echoes and the height of the boundaries of the temperature inversion layer at Oakland, for morning and afternoon. During the morning, lidar observations were made between 10:00 and 11:00 PDT, while during the afternoon, data were collected between 16:00 and 17:00 PDT. The radiosonde data from Oakland referred to 05:00 PDT and 17:00 PDT. All lidar echoes were of the type indicated by the arrows in

---

* It should be noted that only the transmitted radiosonde data were employed in these studies, the original records not being available for analysis. Thus, these data represent greatly smoothed analyses and, of course, noncontinuous temperature and relative humidity profiles.

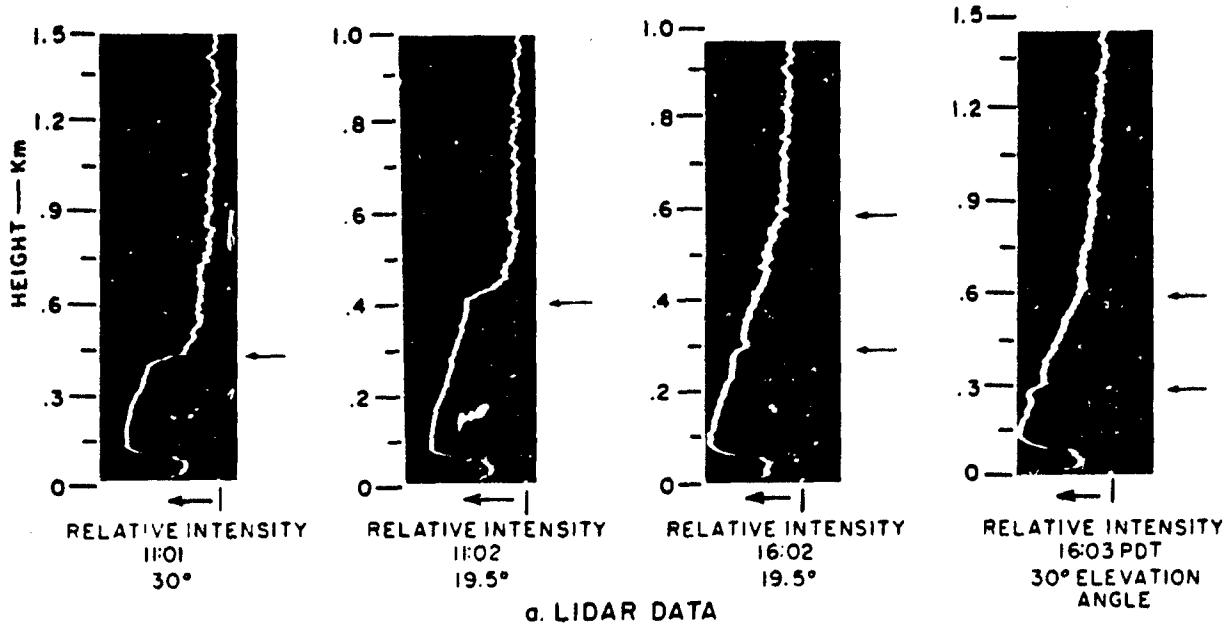

a. LIDAR DATA

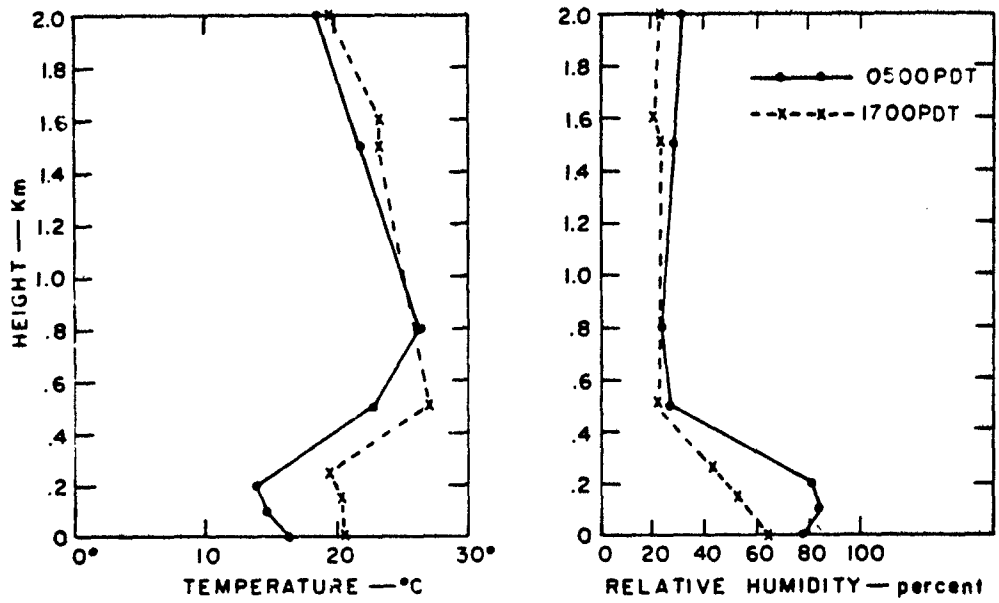

b. RADIOSONDE DATA

FIG. 6 SAMPLE OF LIDAR DATA AND RADIOSONDE DATA FOR 18 AUGUST 1966 — ARROWS INDICATE LARGE CHANGES IN BACKSCATTER

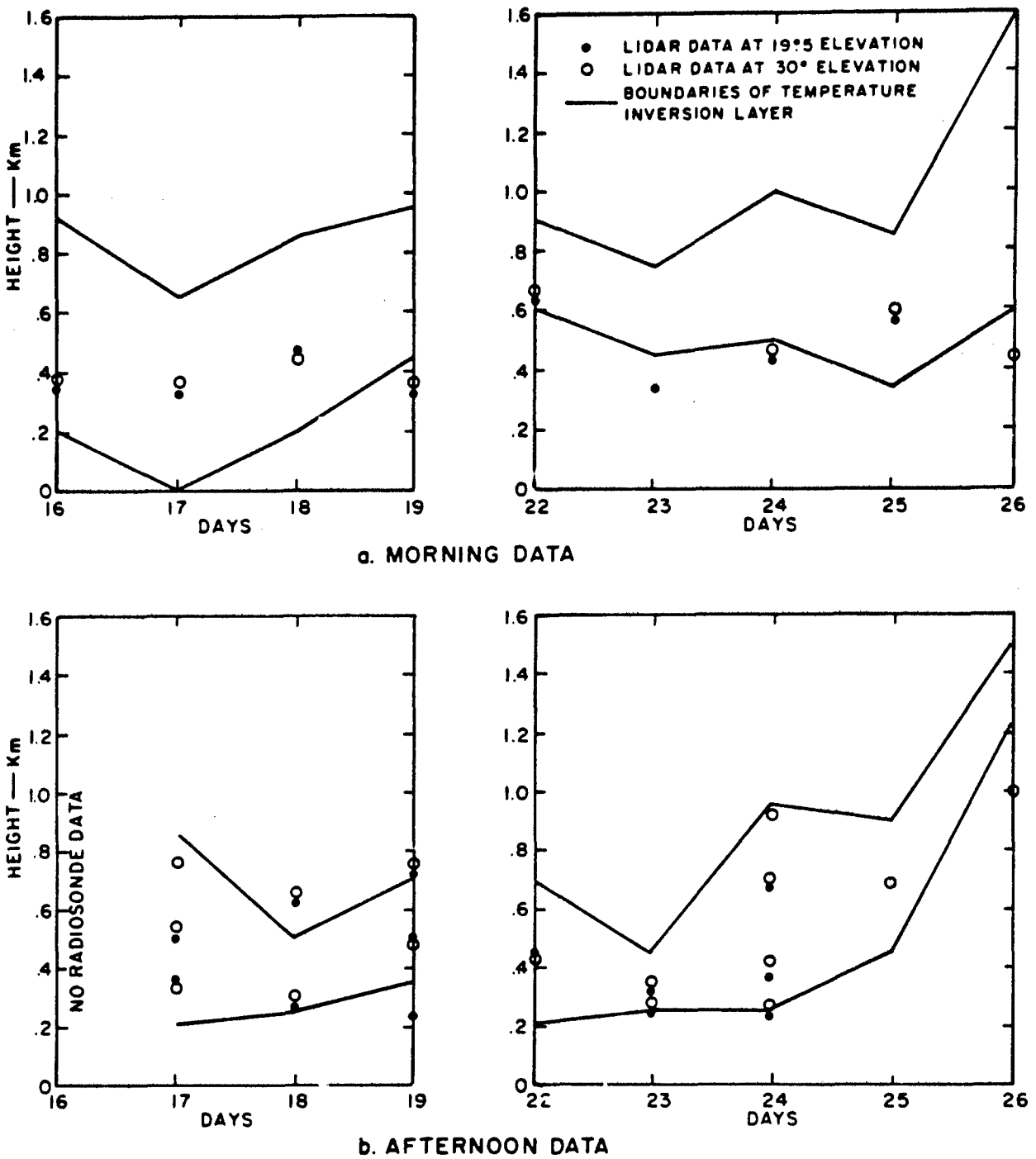

FIG. 7 RELATION BETWEEN THE LOCATION OF OBSERVED LIDAR ECHOES AND THE OAKLAND TEMPERATURE INVERSION LAYER DURING 16 TO 26 AUGUST 1966

the data of Fig. 6a. In Fig. 7a, the sharp decrease in backscatter observed at a single level by the lidar in the morning seems to be related to the lower rather than to the upper boundary of the temperature inversion, except on the first three days of observation. On these days, however, the lower boundary of the inversion was at or very near ground level, so that the difference in time and perhaps location between lidar data and radiosonde data is critical. The rising or lowering of the early morning inversion layer from day to day is sometimes but not always indicated by the lidar data. If the lack of a definite relationship between lidar data and radiosonde data for the morning results from the time differences, then improved relationships should be apparent during the afternoon. In Fig. 7b, the upper and lower boundaries of the inversion layer obtained from the 17:00 PDT radiosonde ascents are compared with the levels at which marked changes in atmospheric backscatter were present in the afternoon lidar data. It is of interest to note that instead of a sharp decrease in backscatter at a single level, the afternoon data invariably show marked changes in atmospheric backscatter at multiple levels. It is seen from Fig. 7b that the lidar echoes are distributed throughout the inversion layer. At times, the lower and upper boundaries are closely approximated by the lidar data. At an elevation angle of 30^{0}, the variation in height of the upper-level lidar echoes is similar to the variation in height of the upper boundary of the inversion.

The data of Fig. 7 show that the variations in atmospheric backscatter observed by the lidar at Menlo Park are only in a general way related to the boundaries of the temperature inversion observed by the radiosonde ascent at Oakland. Periodically, the position of the lower boundary in the morning and the lower and upper boundary in the afternoon can be approximated with the lidar data. The relation between lidar data and temperature data seemed better for the afternoon than for the morning, possibly because of the relatively large difference in time between the morning observations from the lidar and the radiosonde.

No consistent relationship was apparent between the observed lidar echoes and the relative humidity data from the Oakland radiosonde.

The reason for the absence of consistently valid specific relationships between the lidar and radiosonde data may be that the detail in atmospheric structure given by the lidar data is superior to that given by the Oakland radiosonde ascent. Moreover, in dealing with small-scale atmospheric structures, differences in geographic location between places where observations are made may become very important. Oakland is within 20 statute miles of SRI, but the two are separated by San Francisco Bay, which can lead to distinct differences in the atmospheric structure below 1000 m, especially with regard to relative humidity. Oakland is almost directly exposed to air flowing into the basin through the Golden Gate from the Pacific, while air reaching Menlo Park during summer months first flows over a 1000- to 2000-foot-high range of hills.

Since the lidar responds primarily to the vertical structure of the atmospheric aerosol, any relation between the lidar data and the temperature and humidity structure depends on how the latter are related to the aerosol. Thus, a more specific interpretation of lidar data in terms of the vertical structure of temperature and humidity requires measurements from instrumentation that can be launched at the local observation site. Such instrumentation should be able to measure the vertical structure of the temperature and humidity as well as that of the aerosol on a scale comparable to that provided by the lidar data. An instrument package with simultaneous temperature and relative humidity readouts attached to a tethered balloon seems most desirable.

The spatial extent of atmospheric structure that can be obtained with the lidar, using elevation angles ranging from 5° to 75°, is illustrated in Fig. 8 for 26 August 1966. Spatial variations in atmospheric backscatter observed by the lidar are plotted on a horizontal-range versus altitude scale. Observations were made while scanning from NNW to SSW. The results indicated are those from two complete scans made during the morning and two complete scans made during the afternoon.

It can be seen that distinct boundaries between atmospheric layers of different lidar response can be analyzed. Two boundaries are present in the morning, one near 500 m and the other near 1000 m. The upper one is most pronounced when viewing NNW. During the afternoon, the boundary at 1000 m has intensified but the boundary that was observed at 500 m in the morning has disappeared. It is believed that the data of Fig. 8 reflect the changes in the vertical distribution of the aerosol that are due to changes in the thermal stability of the atmosphere from morning to afternoon. In the afternoon, the 1000-m boundary, indicated by the lidar data, may correspond to the top of the turbulent mixing layer. The transient lidar echoes observed below 1000 m are of the type classified as angels in radar data.

3. Radar Data

Data from the K_a-band microwave radar obtained for 26 August 1966 are shown in Fig. 9. Two one-minute time sections of the film strips on which radar echoes were recorded are shown. During the morning, the radar-echo pattern resembled that of angels. All echoes were observed below 750 meters. During the afternoon, strong echoes continuous in time were recorded up to about 1000 m, with occasional weaker echoes present above this level. It is of interest to note that the continuous radar echoes appeared below the 1000-m boundary identified by the afternoon lidar data in Fig. 8. More details of the lidar and radar echoes observed during the afternoon can be obtained from a sample of the traces of signal intensity versus height shown in Fig. 10.

The lidar traces refer to an elevation angle of 75^0 and the radar traces to an elevation angle of 90^0. Many similarities between the lidar and radar data are evident. For example, the radar data show continuous echoes near and below 1000 m, which is the level at which the lidar indicates a sharp decrease in atmospheric backscatter. A smaller change in atmospheric backscatter as observed by the lidar is apparent near 1500 m. The location of both changes in backscatter are indicated by arrows in Fig. 10. Occasional weak radar echoes near 1500 m can be seen

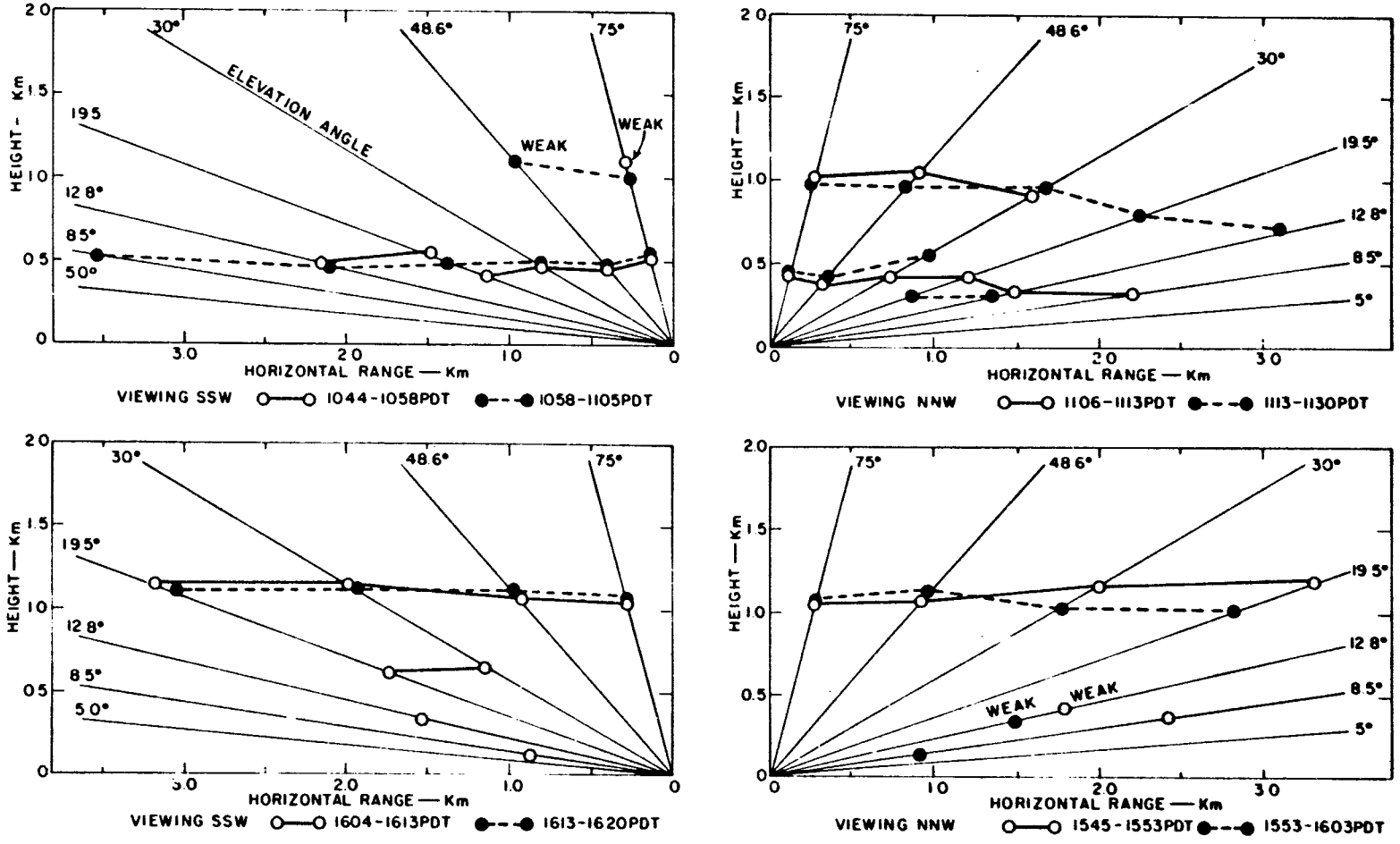

FIG. 8 ATMOSPHERIC STRUCTURE ANALYZED FROM LIDAR DATA (solid and open circles) AT ELEVATION ANGLES RANGING FROM 5° TO 75°, 26 AUGUST 1966

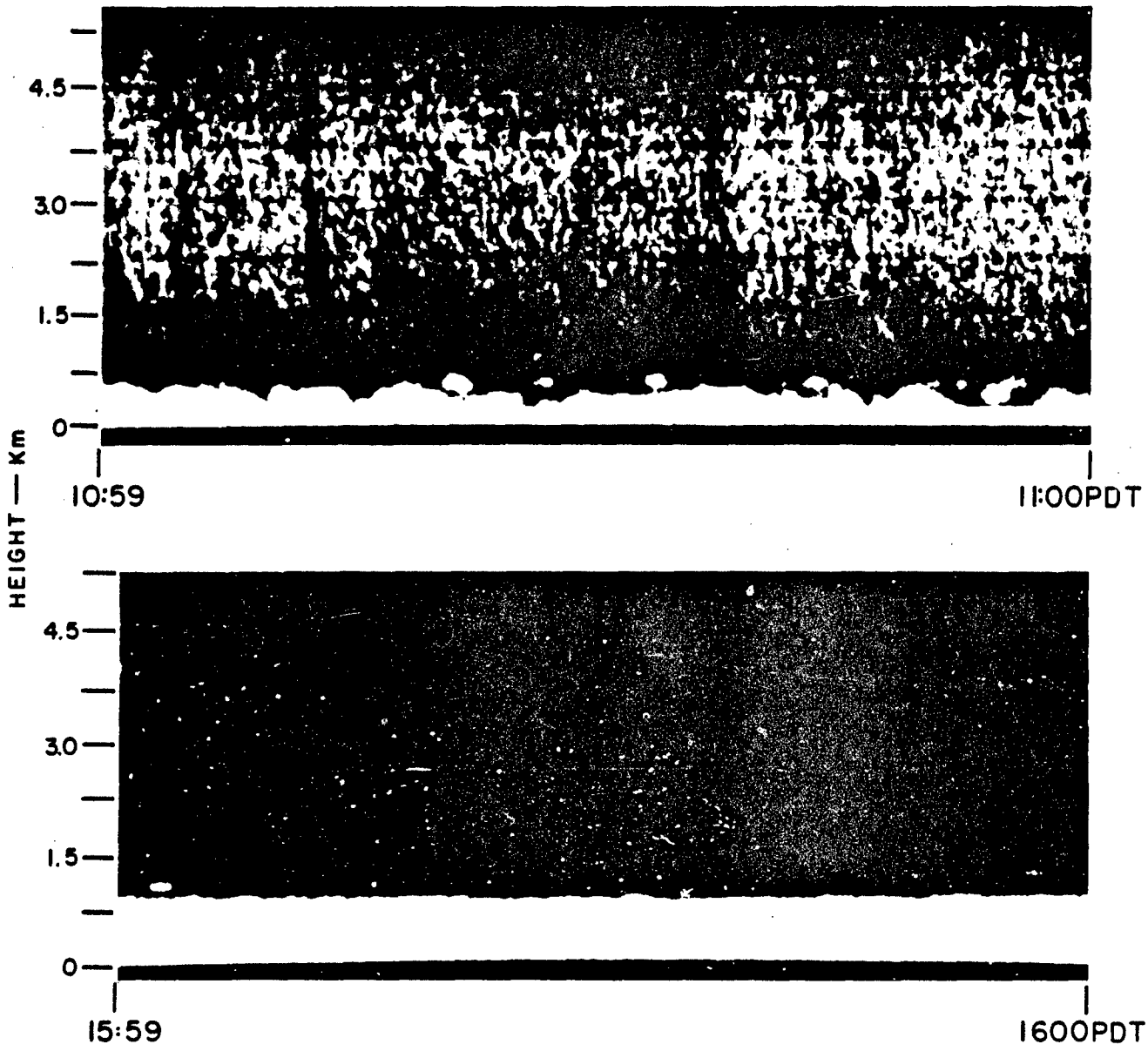

FIG. 9 SAMPLE OF FILM-RECORDED RADAR DATA FOR 26 AUGUST 1966

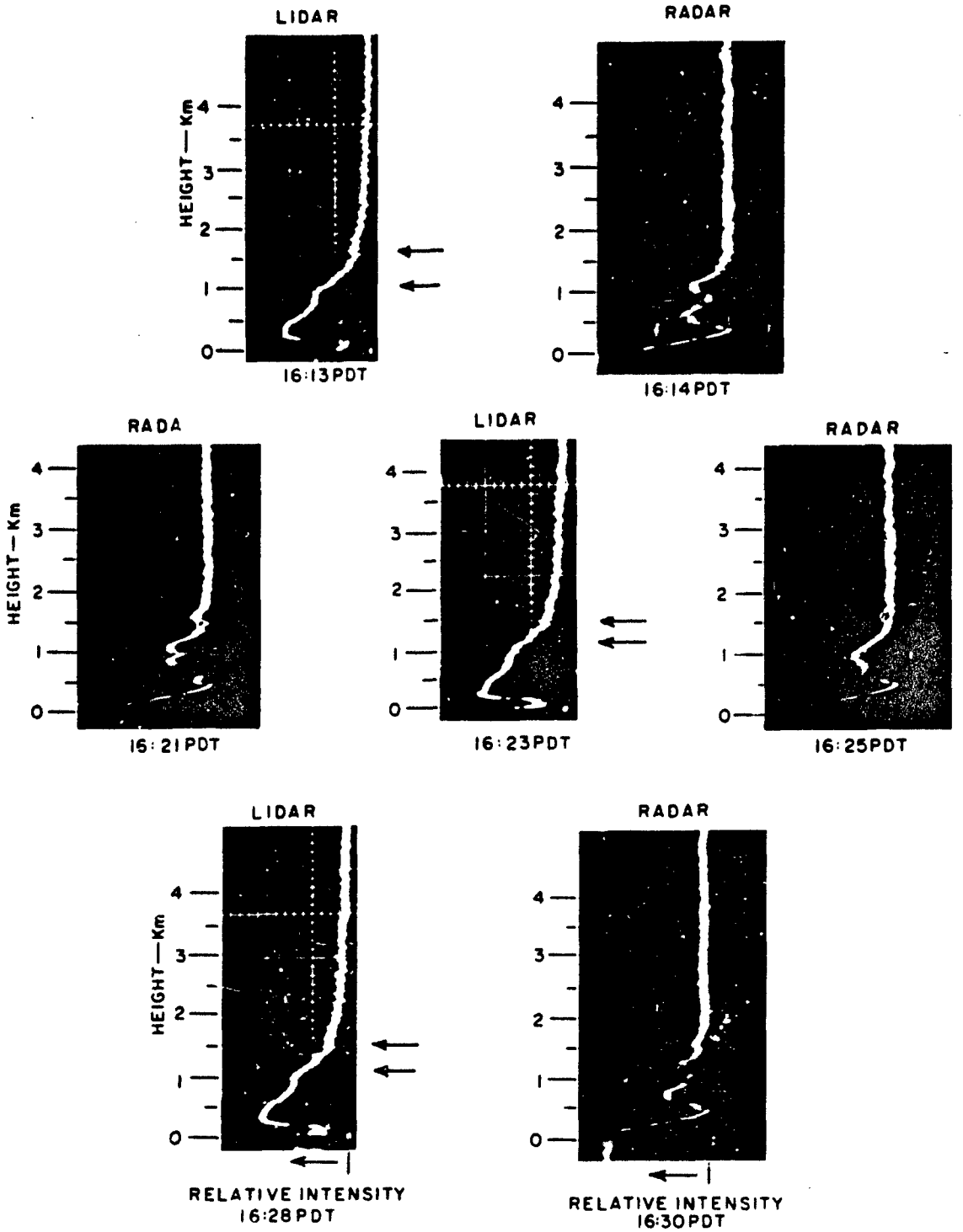

FIG. 10 TRACES OF SIGNAL INTENSITY VERSUS HEIGHT FROM RADAR AND LIDAR OBSERVED ON AFTERNOON OF 26 AUGUST 1966 — ARROWS INDICATE LARGE CHANGES IN BACKSCATTER OBSERVED WITH LIDAR

in the film data of Fig. 9 and in the traces of Fig. 10. These weak radar echoes seem to correspond to the second (1500 m) change in backscatter indicated by the lidar.

To what extent the lidar and radar echoes describe the same physical phenomenon could not be determined. If the 1000-m boundary identified by the lidar data during the afternoon is the upper boundary of the turbulent mixing layer, it can be postulated that convection and turbulence were major contributors to the presence of the radar echoes. While the meteorological discontinuities observed by the lidar may well give rise to the dielectric inhomogeneities postulated by some as the source of radar echoes, the data are not wholly incompatible with returns from insects, which may equally well be expected to occur in concentrations related to the atmospheric discontinuities. At this time it is unknown how similar or dissimilar the ruby lidar and K_a-band radar would respond to a given aerosol stratification.

C. OBSERVATIONS DURING THE PERIOD 14 SEPTEMBER THROUGH 15 SEPTEMBER 1966

On 14 and 15 September 1966, observations were made to investigate diurnal variations in the lidar and radar echoes observed below 2000 m. For periods up to 12 hours, both the ruby and neodymium lidars were fired at intervals of 1 to 3 minutes. Elevation angles ranged from 19° to 75°. The radar, pointing vertically upward, was operated continuously.

The only clouds observed during the period were scattered cirrus that moved rapidly through the local area during the afternoon of 14 September. At ground level the horizontal visibility was generally above 10 miles. Only during early morning and later afternoon did the visibility decrease somewhat due to haze and/or smog.

A sample of the traces of the logarithm of the signal intensity versus height obtained from the ruby and neodymium lidars is shown in Fig. 11 for four different times on 14 September 1966. Because of lower receiver sensitivity, our neodymium lidar is not as effective an indicator of atmospheric structure as our ruby lidar. Of course, differences in atmospheric backscatter at the two wavelengths involved

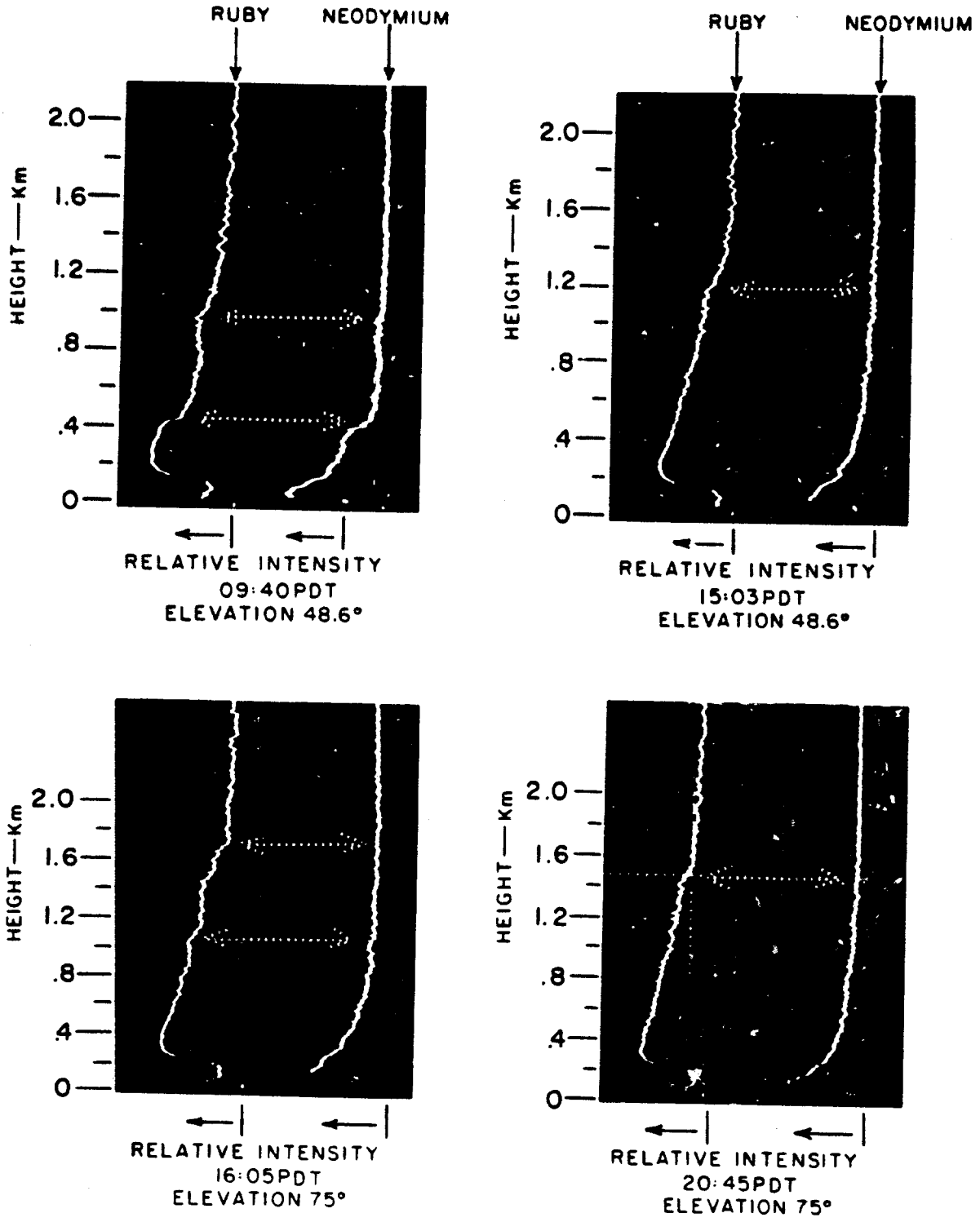

FIG. 11 TRACES OF SIGNAL INTENSITY VERSUS HEIGHT FROM RUBY LIDAR AND NEODYMIUM LIDAR, 14 SEPTEMBER 1966 — ARROWS INDICATE LARGE CHANGES IN BACKSCATTER

(0.6943μ and 1.06μ) may also be a factor. It can be seen (see arrows in Fig. 11) that distinct changes in atmospheric aerosol at one or more levels are indicated by the traces for the ruby lidar at all four times, but only at one time (09:40 PDT) by the traces for the neodymium lidar.

In Fig. 12, the heights of changes in atmospheric backscatter observed with the ruby lidar during the period 14/0900 to 15/0000 are plotted as a function of time. The data refer to an elevation angle of about 49°. Echoes that were identifiable in time are joined by straight lines in order to emphasize the time dependence of the height variations. At the beginning of the observation period (14/0900), two echoes were distinguished--one located between 400 m and 500 m, and the other located around 1000 m. These two changes in atmospheric backscatter gradually descended in height and finally disappeared from the lidar traces near 12 o'clock. Due to an equipment problem no observations were made between 12 o'clock noon and 13:40 PDT When observations were resumed, only a single lidar echo was observed between 1300 and 1400 m. At midafternoon, however, echoes began to appear at various levels up to 1500 m. Figure 12 shows a large height variation with time of the observed changes in backscatter above 1000 m.

It is of interest to note that the changes in height of the lidar echoes observed above 1000 m during the afternoon are very similar to the large changes in humidity found by Zobel [1966] near the base of a subsidence inversion. Zobel postulated that the large changes in humidity may have been due to variations in the height of the inversion layer or by vertical air currents in places where convection penetrated the inversion. The height variations observed in the lidar echoes for the afternoon can be explained in a similar way, since changes in height of the inversion and vertical air currents can both affect the aerosol distribution. Below 1000 m, lidar echoes could not always be clearly identified, and therefore the indicated height variations are uncertain. The lowest echoes were similar to those observed below 1000 m on the afternoon of 26 August 1966 (see Fig. 8); they could not be followed continuously in time and resembled what is commonly referred to as

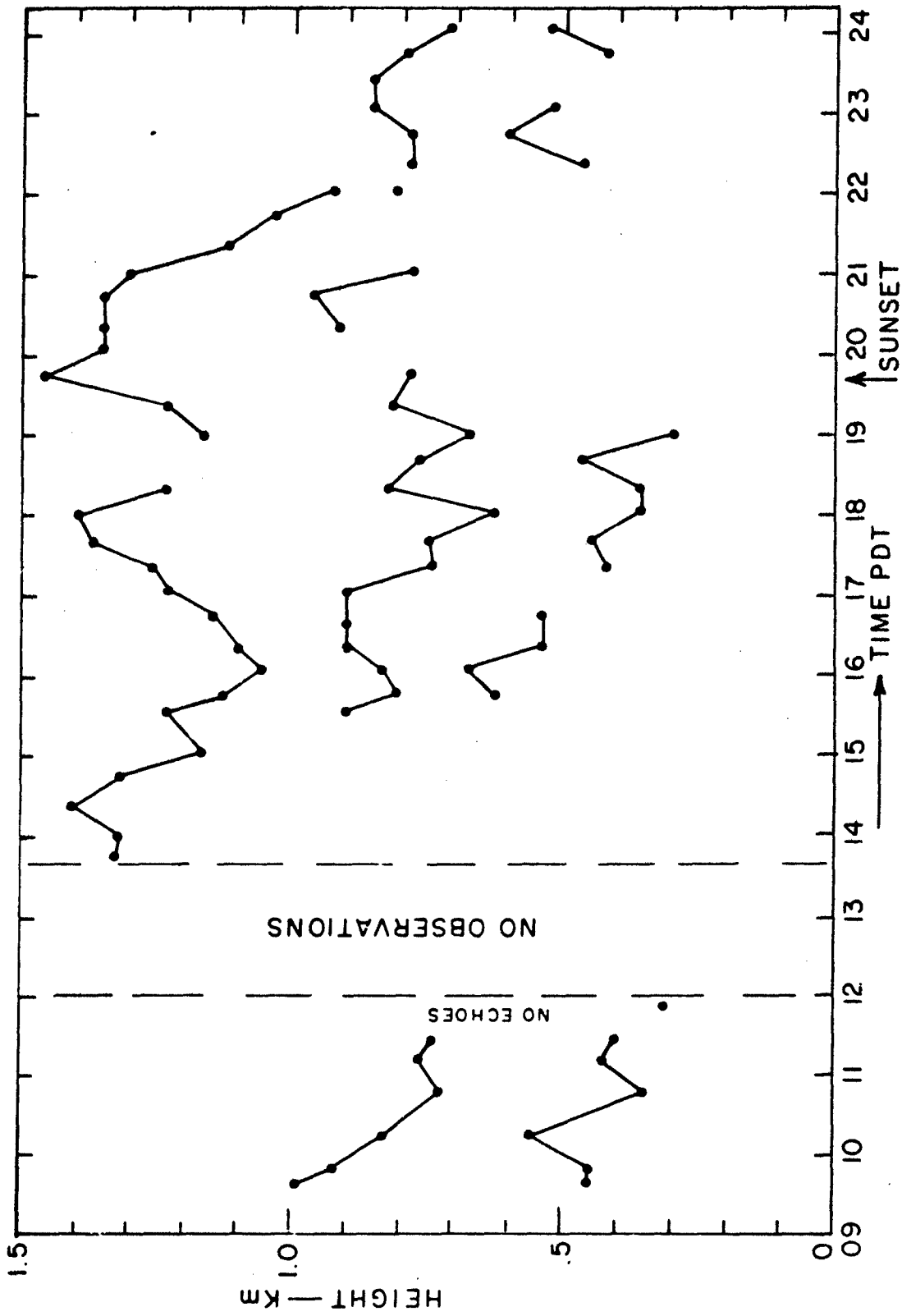

FIG. 12 HEIGHT AND HEIGHT VARIATION OF LIDAR ECHOES OBSERVED ON 14 SEPTEMBER 1966

angel activity in radar. During the evening, the observed changes in atmospheric backscatter began to converge toward lower levels, and by about 22:00 PDT, all echoes above 1000 m had disappeared. Thus, the lidar data of Fig. 12 reflect the daily march of the thermal stability of the atmosphere.

Using the pibal data from nearby Oakland for the same day, vertical profiles of the magnitude of the vertical wind shear vector and the turning of the wind with height were computed. Above 1000 m, a large increase in these quantities from morning to afternoon was found. No specific connection between the multiple layers of lidar echoes observed during the afternoon and early evening and the vertical wind shear was apparent.

In order to investigate further the time-dependent changes in height of the lidar echoes apparent in Fig. 12, observations were continued on 15 September. At 0500 PDT, before sunrise, a sharp decrease in backscatter, observed at 200 m, marked the upper boundary of the local marine layer. Using an elevation angle of 19.5^{0}, the height of this upper boundary was mapped with the ruby and neodymium lidars for a period of nearly 7 hours. Results for the ruby lidar are illustrated in Fig. 13. The inset shows the upper boundary as it was identified in the traces of signal intensity versus height. It can be seen that twice during the 7-hour observation period the upper boundary descended in height, disappeared, and reappeared. Such height oscillation must arise from time-dependent variations in the vertical distribution of the aerosol. Since convection had not developed to its maximum intensity, it is postulated that the data of Fig. 13 reflect variations in the height of the inversion layer. The Oakland radiosonde ascent showed an early-morning inversion layer with a lower boundary at ground level and an upper boundary near 500 m.

Figure 14 shows samples of the radar echoes that were obtained on 14 September 1966 for the same period during which the lidar data of Fig. 11 were collected. The samples are one-minute sections of the film strips on which the radar echoes were recorded. The discrete

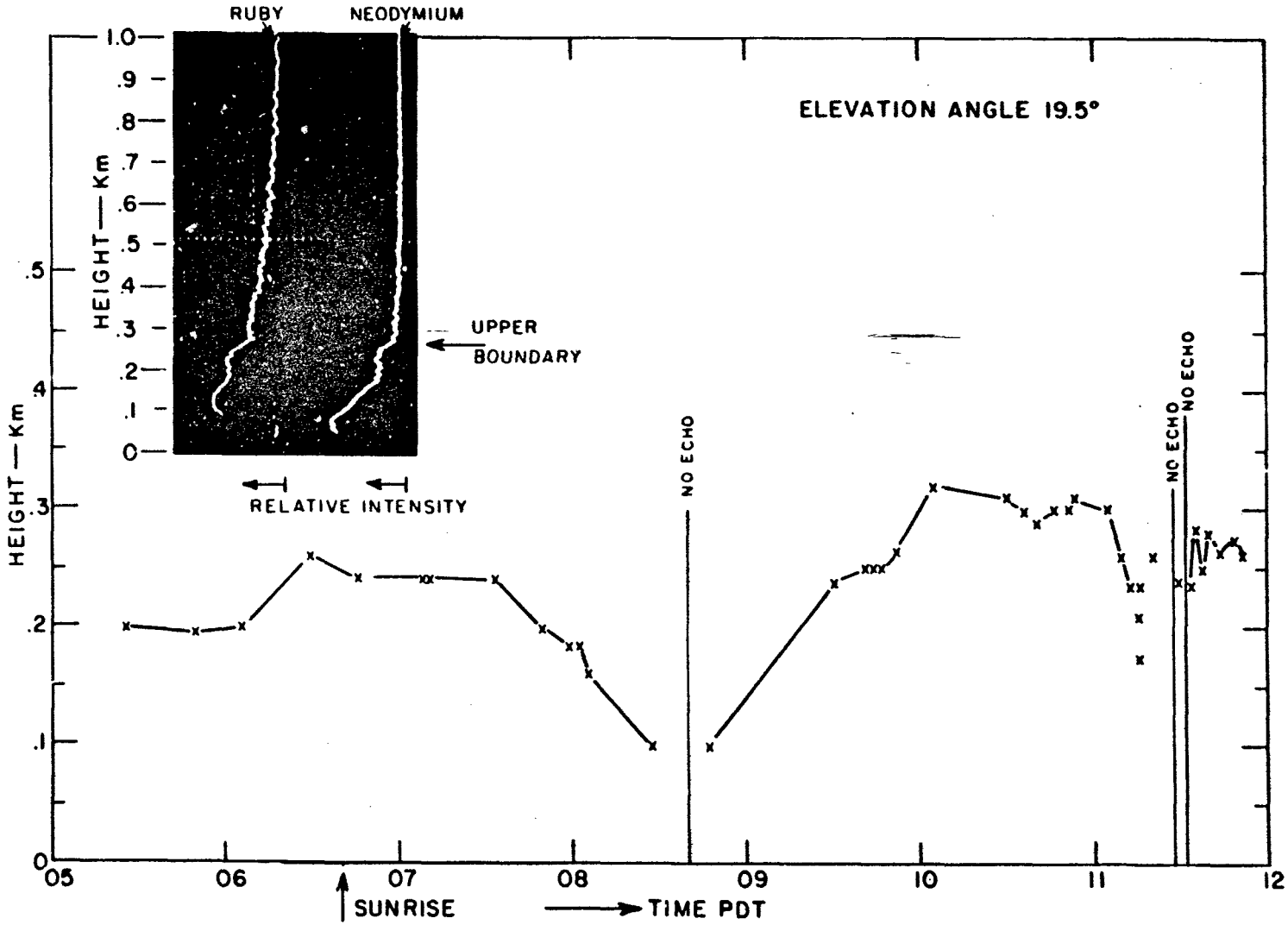

FIG. 13 HEIGHT VARIATION OF UPPER BOUNDARY OF LOCAL MARINE LAYER AS OBSERVED BY LIDAR ON 15 SEPTEMBER 1966. Inset: sample of traces of signal intensity versus height from ruby and neodymium lidar observed at 06:28 PDT

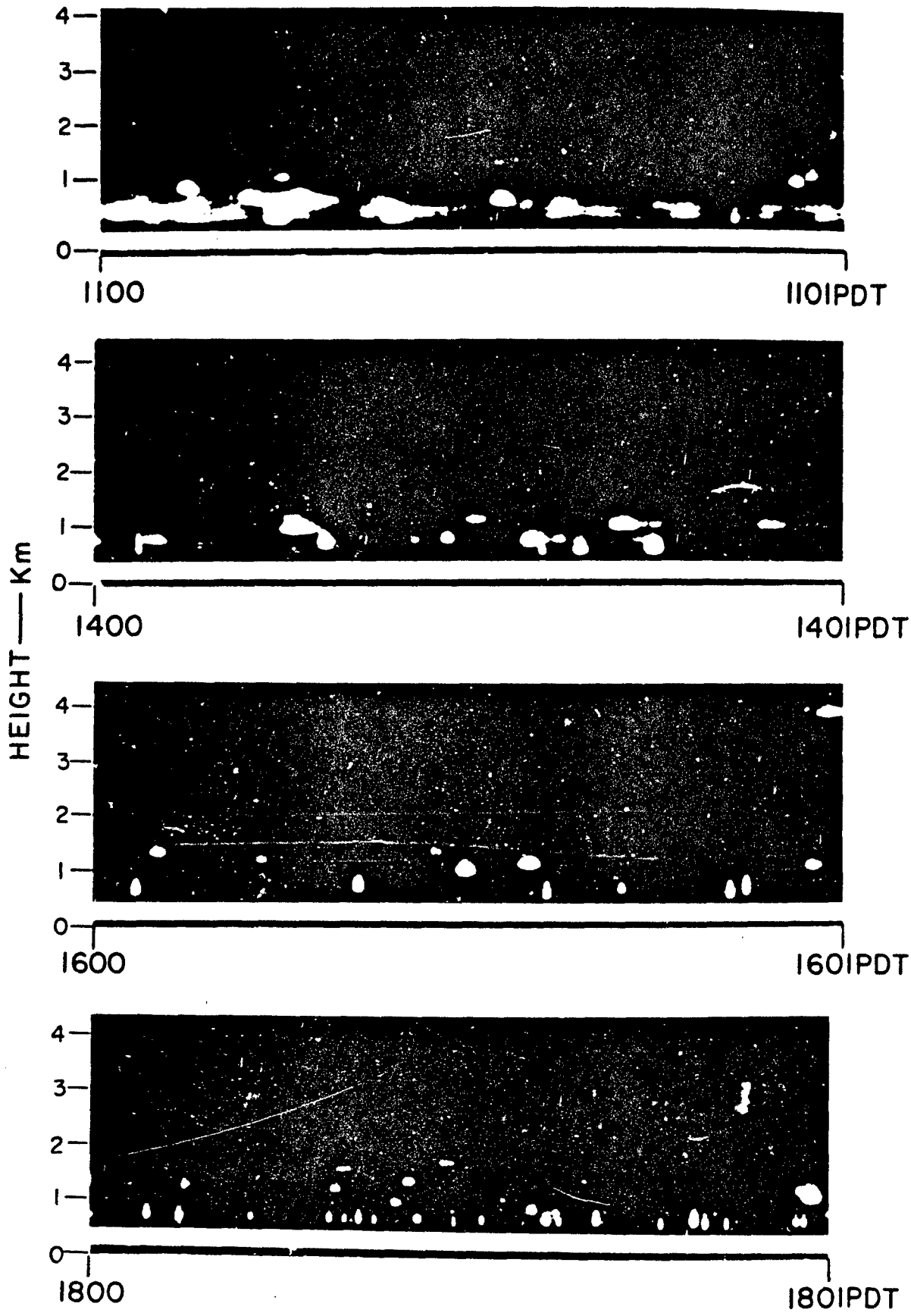

FIG. 14 SAMPLES OF RADAR ECHOES, FI

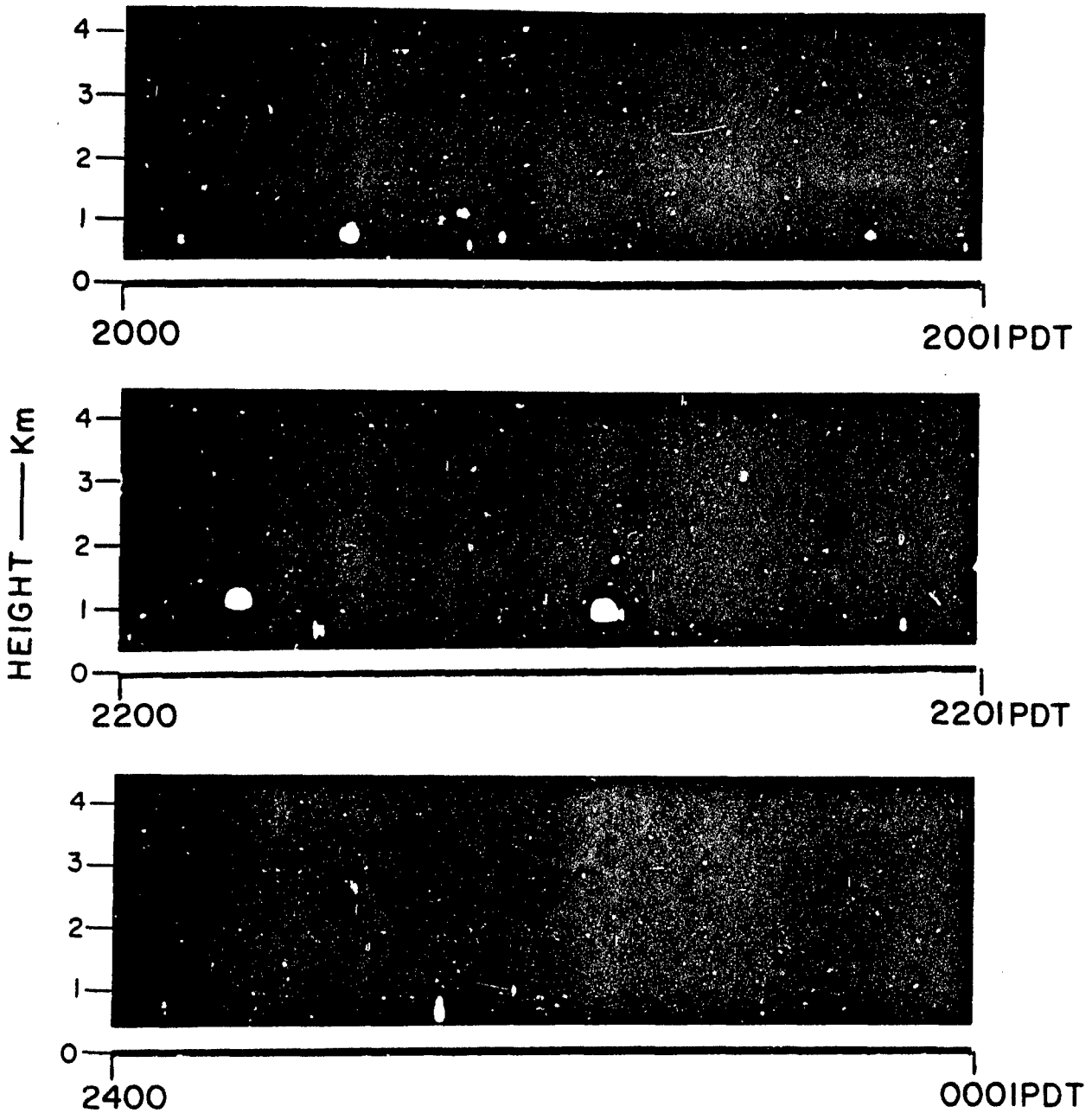

S, FILM-RECORDED ON 14 SEPTEMBER 1966

FIG. 14

B

echoes observed below 2000 m are meteorological angels. They occurred most frequently during the late afternoon (18:00 PDT) and practically disappeared toward midnight. The radar echoes observed during the morning of 15 September (not shown) had a similar pattern: At 06:00 PDT only occasional discrete echoes were recorded below 2000 m, but the frequency of occurrence of these echoes increased rapidly toward 12 o'clock noon. The time changes observed in the frequency of occurrence of the radar echoes shown in Fig. 14 strongly suggests a connection with the thermal stability of the lower atmosphere and the surface temperature which is similar to that shown by Planck [1956] for the 1.25-cm radar. The lidar data of Fig. 12 show a similar connection with the thermal stability.

On the other hand, the steady increase in the number of discrete radar echoes that was observed on 15 September between 0600 PDT and 12 o'clock noon had no obvious relation to the time-dependent variation in height of the upper boundary of the marine layer present in the lidar data of Fig. 13. Thus, there was no consistent relationship between the lidar data and the radar data. The atmospheric structure analyzed from the lidar data was coherent and appeared to represent the vertical structure of the aerosol. The radar data resemble angel activity, with a strong dependence on surface temperature.

IV OPTIMUM CHARACTERISTICS OF A LIDAR LOWER-ATMOSPHERE PROBE

A. INTRODUCTION

A discussion of the optimum characteristics of an instrument suitable for indirect measurement of temperature, humidity, or wind in the lower atmosphere is not possible at this time, because the present study was unable to isolate the individual contributions of these three variables to the total backscattered signal. In the event that routine observations of the lower atmosphere such as discussed in this report are desired, various improvements in the equipment can be recommended. The optimum characteristics of a lidar suitable for such observation are discussed in this section. These characteristics are based on the operational experience gained during this study.

The determination of optimum system parameters is based on the lidar equation (1), which must be modified slightly to describe the backscattered return from a clear atmosphere:

$$P_r = P_t \frac{A_r}{R^2} \frac{1}{4\pi} \frac{C\tau}{2} \beta'_{180}(R) T_o \exp\left[-2 \int_o^R \sigma dR\right] , \qquad (3)$$

where R is the one-way distance to the scattering volume* in question, and $\beta'_{180}(R)$ and σ are functions of range R. Equation (3) is valid in the region of R, extending from the minimum range (where the receiver field of view completely intercepts the transmitted beamwidth) to the range at which P_r approximately equals the receiver noise power P_n.

Noise power P_n is determined by either the solar radiation scattered into the receiver field of view, or by the detector noise level, whichever is greater. For most receiver designs, the former condition usually

---

* The scattering volume (a truncated cone) is defined by the beamwidth of the transmitted radiation and half the transmitted pulsewidth.

prevails in the daytime and the latter condition at night. The receiver noise power produced by solar radiation is given by:

$$P_n = \frac{\pi}{4} N_\lambda \theta^2 A_r (\Delta\lambda) T_r \qquad (4)$$

where

N_λ = Radiance of the clear sky at the wavelength of interest (Watts cm^{-2} $steradian^{-1}$ Å^{-1})

θ = Receiver field of view (rad)

$\Delta\lambda$ = Wavelength interval of the predetection filter (Å)

T_r = Transmission efficiency of the receiver optics.

The receiver noise power produced by detector noise is determined by the input power level corresponding to the dark current of the specific detector used.

The following parameters may therefore be manipulated in order to maximize Eq. (3) and minimize Eq. (4): P_t, A_r, τ, T_o, θ, $\Delta\lambda$, and detector noise level. Many of these parameters interact with each other and cannot be independently specified; the final choice represents the best compromise for the given application of the equipment. The optimum values of the remaining parameters may be determined by consideration of the various trade-offs available. System parameters which primarily influence data display and recording are discussed later in this section.

B. SELECTING THE MAJOR PARAMETERS

1. Choice of Laser Material

Although laser material does not appear directly in the above discussion, the choice of a laser source places restrictions on transmitted power (P_t), wavelength (λ), pulselength (τ), and the repetition rate. The selection of a particular operating wavelength, in turn, places limits on the choice of available detectors, which may influence system sensitivity. In order for a lidar to obtain a useful maximum range and good range resolution, the choice is limited to laser sources capable of

producing high peak-power outputs and relatively short pulse lengths.* At the present time, these selections are: ruby (0.6943μ), neodymium (1.06μ), and the second harmonic of neodymium (0.53μ).

a. Ruby Laser

A Q-switched† ruby laser is capable of producing peak-power outputs of 10^7 to 10^8 Watts with pulse lengths of 30 ns. The typical repetition rate of an air-cooled ruby laser is 2 to 4 ppm. Significantly higher repetition rates (up to 1 pps at 10^7 Watts peak power) are possible by liquid-cooling the ruby rod and flashlamp. Because the laser power supply and ruby cooling requirements increase rapidly with increasing repetition rates, the cost of a ruby laser system increases drastically for pulse repetition rates in excess of 4 ppm.

b. Neodymium Laser

A Q-switched neodymium-doped glass laser (1.06μ) can operate at higher repetition rates (12 ppm) and can produce greater peak output powers, with pulselengths comparable to the ruby device. As with the ruby laser, the pulse repetition rate can be further increased by liquid cooling. The most serious drawback of a neodymium lidar is the lack of an adequate detector having a high quantum efficiency and low noise level at 1.06μ.

The low-quantum efficiency and high noise level of the detector reduces the overall sensitivity of the equipment to below that of a comparable ruby lidar. This reduction in sensitivity more than offsets

---

* The variations of extinction coefficient and backscatter coefficient with wavelength are secondary considerations here.

† A ruby laser operating in the long-pulse mode is capable of producing considerably more output energy than the Q-switched laser. However, the pulse length obtainable from a long-pulse laser is in the order of several hundred microseconds. In addition, the output is not a smooth, gaussian-shaped pulse, but tends to be very ragged and non-uniform in amplitude. Because of the poor range resolution obtainable with long-pulse lasers, these sources are not considered further in this report.

any gain obtained with the somewhat increased transmitter power available from the neodymium laser. The effect of detector performance on the selection of operating wavelength is discussed later in this section.

c. Neodymium--Second Harmonic Laser

A more favorable match between laser output wavelength and detector sensitivity can be obtained by utilizing the second harmonic of neodymium glass (0.53μ). This wavelength is obtained by inserting a nonlinear optical element [such as potassium dihydrogen phosphate (KDP)] into the output beam of a neodymium glass laser. The major drawback of this optical configuration lies in the low conversion efficiency of the KDP crystal (15 percent). System calculations and recent experiments at SRI with a lidar operating at 0.53μ showed no clear-cut advantage of this wavelength over ruby for the kind of application discussed here.

For this application, the high power output, simplicity, good detector quantum efficiency, and relatively low cost of a Q-switched ruby laser seem to outweigh its low pulse repetition rate. Moreover, the disadvantage of low repetition rate may be eased by proper choice of data recording instrumentation.

2. Pulse Length(τ)

Although longer pulse lengths may be desirable, the selection of a Q-switched ruby laser presently restricts the output pulse length to the interval between 25 and 40 ns. The corresponding range resolution of 3.75 to 6 m seems to be more than adequate for most meteorological work.

3. Laser Transmitter Power Output (P_t)

As discussed earlier, all the significant information contained in the return signal from the clear atmosphere occurs in that region between the minimum range of the equipment and the range at which the backscatter return from the clear air approximately equals the receiver noise level. These ranges correspond to 0.3 km and 1.6 km, respectively, in Fig. 11 (ruby).

The maximum range of the optimum lidar should therefore extend to the maximum height of meterological interest. For this application (as discussed in Section I) the maximum is approximately 2 km. System calculations verified by experiment show that a transmitter peak power of 20 MW will be adequate to receive clear-air backscatter returns from a height of 2 km.

4. Temperature Dependence of Ruby Output Wavelength

Abella and Cummings (1961) have reported the ruby temperature coefficient of wavelength as +0.065 Å/°C, in the temperature range of 25°C to 80°C. Unless a spectral scanning lidar is desired, close regulation of the ruby operating temperature is not required, except to ensure that the ruby output wavelength does not drift into the atmospheric water-vapor absorption line centered at 6943.8 Å (Long and Boehnker, 1965). This wavelength occurs at a ruby temperature of 36.5°C.

5. Transmitter Beamwidth and Receiver Field of View (θ)

For most applications, the transmitter beam divergence is made as small as practicable for compatibility with the receiver field of view, which itself must be minimized because of receiver noise considerations [see Eq. (4)]. A transmitter beam divergence of 0.5 mrad is easily attained with 6-inch diameter optics. The resulting spatial resolution of one meter at a range of 2 km seems adequate for this application.

A receiver field of view approximately two times greater than the transmitter beamwidth will considerably ease the requirement of maintaining an accurate optical alignment between transmitter and receiver over normal temperature variations. A receiver with an adjustable field of view is desirable for nighttime observations, where the receiver field may be enlarged considerably to reduce the minimum range of the equipment without increasing the receiver noise level. Since P_n is proportional to θ^2 in Eq. (4), it is advantageous to reduce the receiver field of view to a minimum during daytime operation. This minimum value is determined by the thermal stability of the transmitter and receiver optical axis alignment.

6. Receiver Aperture (A_r)

Commercially available six-inch diameter Newtonian optics (approximately 180 cm^2 effective aperture area) provide the advantage of an adequate receiver aperture in a smaller physical size and at lower cost than equivalent refractive optics.

The disadvantage of reflective optics lies principally in the sensitivity to thermal effects on mirror alignment and the difficulties of making a sufficiently rigid mounting.

7. Optical Transmission (T_o)

The transmission of refractive optics and the reflectivity of mirrored surfaces can be as high as 0.95 per element at ruby wavelength. A typical value of transmission for the predetection filter is approximately 0.50 (the exact value is influenced by the choice of other filter parameters). The total value of optical transmission for the lidar discussed here is approximately 0.36.

8. Predetection Filter Wavelength Interval ($\Delta\lambda$)

For daytime operation, the ruby lidar receiver noise level is usually determined not by the detector noise level, but by solar radiation scattered into the receiver field of view. Two methods are used to reduce this solar noise level: one is to minimize the receiver field of view, the other is to insert a narrow-band interference filter into the optical path directly ahead of the detector. The passband of the interference filter is usually centered at the nominal ruby wavelength; the wavelength interval of the filter is determined by both the expected wavelength change of the laser output due to temperature, and also by the temperature coefficient of wavelength of the filter (a typical value of filter temperature coefficient is +0.35 Å/°C). A filter wavelength interval of 12 Å will be adequate for operation over normal temperature variations.

In addition, the filter stop band should be broad enough to block all wavelengths within the spectral response of the detector.

9. Detector

The fast response time, high gain, and high sensitivity of the photomultiplier make it an ideal detector for laser wavelengths in the visible portion of the spectrum, and out to approximately 1μ. Beyond 1μ, photoemissive detectors gradually become ineffective because of decreasing quantum efficiency. Photoconductive detectors must be used at wavelengths greater than 1.1μ.

In addition to spectral response characteristics, an important consideration regarding the selection of a detector is the internal noise levels of the various devices. The internal noise level is a function of the type of cathode material, the cathode area, and the temperature. In general, detectors employing an S-20 photosurface tend to have internal noise levels 1 to 2 decades lower than tubes employing S-19 photocathodes, and 3 to 4 decades lower than S-1 photocathodes. For ruby lidars, the use of photomultiplier with an S-20 photocathode results in a detector noise level lower than the background noise level produced by solar radiation.

A photomultiplier gain of approximately 10^6 will produce a video signal suitable for direct input into electronic recording or data processing equipment.

10. Lidar Mounting

The entire optical assembly (consisting of laser, optics, detector, etc.) should be mounted on a platform which is capable of being positioned from 0° to 90° in elevation and 360° in azimuth, so that observations may be taken at any angle above the horizon.

C. SYSTEM PARAMETERS DIRECTLY INFLUENCING THE LIDAR DATA

1. Post-Detection Filter Bandwidth

The post-detection filter bandwidth (usually incorporated into the characteristics of a video amplifier following the detector) determines the range resolution obtainable from the lidar. Although 35 MHz bandwidth is necessary to realize the 4.5-m range resolution inherent in a 30-nanosecond transmitted pulse, range resolutions this small are not

always required. For example, Fig. 13 shows lidar returns obtained with a post-detection filter bandwidth of 6 MHz. The corresponding range resolution of 20 m seems adequate for clear air observations.

2. Video Amplifier

Because of the large amplitude range of signals present on any one lidar return, a method of displaying both very large and very small signals simultaneously is desirable. A logarithmic video amplifier of bandwidth sufficient to provide the desired range resolution is a convenient means of obtaining this compression. The dynamic range of the amplifier should be compatible with the linear range of the photomultiplier output. Typically, dynamic ranges of 3 to 4 decades are adequate.

3. Data Recording

Until recently the only satisfactory method of recording lidar returns was to photograph an oscilloscope display in the form of a conventional radar A-scope. A cathode ray tube with P-11 phosphor and Polaroid 410 or Kodak 2475 film performed very satisfactorily.

An Institute-sponsored program to develop techniques of lidar recording and display has shown that certain forms of magnetic recording will prove valuable. The recording of the lidar video signal on a rapidly rotating magnetic disc, and the subsequent repetitive readout of the same signal at 30 times a second, has significantly reduced the disadvantage of a low repetition rate of the laser. In addition, up to 500 lidar observations can presently be stored on each side of the disc.

4. Lidar Repetition Rate

The choice of a ruby laser source establishes some general limits on the repetition rate of the lidar. However, the main limitations are the high cost and mechanical complexity of liquid-cooled, high repetition rate systems. Since the time scale involved in clear air observations is rather long, a lidar pulse repetition rate of 3 ppm will provide a marginally low data rate for a lidar system when overall equipment cost is an important factor.

D. CALIBRATION AND PERFORMANCE MONITORING

The well-known techniques used in the calibration of microwave radars (such as measurements of transmitted power and receiver sensitivity) are presently difficult to implement at optical frequencies because of the lack of adequate instrumentation.

The following method provides a means of calibrating the lidar and monitoring its performance. The method makes use of an optical arrangement to sample a small, fixed percentage of each transmitted pulse, attenuate the pulse by a known amount, and insert this attenuated pulse into the receiver. Since the transmitted power has been measured previously, the height of the reference pulse occurring at zero range is a convenient indication of the absolute power level at the receiver. The reference pulse provides a convenient monitor of system performance, since any gradual degradation of transmitter output or receiver sensitivity is indicated by a decrease in the reference pulse amplitude. The reference pulse can also be used to eliminate variations in the received data produced by pulse-to-pulse variation in the transmitted power. An absolute measure of return signal amplitude is made by comparing the height of the return signal with the height of the reference pulse.

E. THE PROPOSED OPTIMUM SYSTEM

Table III summarizes the optimum lidar characteristics, the details of which have been discussed above. The suggested characteristics represent what is considered to be an optimum solution that can be achieved at this time with reasonable expenditure of time and funds. Several limitations inherent in this system are discussed below, and means of reducing their significance are suggested.

1. Maximum Range

Although it is believed that the maximum range of 2 km is adequate for the conditions encountered in Menlo Park, California, this maximum range may not be adequate elsewhere. The simplest way to increase the maximum range at which returns from the clear atmosphere can be detected

Table III

OPTIMUM LIDAR CHARACTERISTICS

	Lower Limit	Probable Selection	Upper Limit
Transmitter			
Laser Material		Ruby	
Wavelength (Å)		6943	
Peak Power (Watts)		2×10^7	5×10^7
Pulse Length (ns)	25	30	40
Optics		6-inch reflector	
Beamwidth (mrad)		0.5	1.0
Firing Rate (ppm)			
Air-cooled	1	3	4
Liquid-cooled		60	60
Receiver			
Optics		6-inch reflector	
Field of View (mrad)	0.8	1	3
Predetection Filter Wavelength Interval (Å)	12	12	15
Detector		Photo-multiplier S-20 Cathode	
Post-Detection Filter Bandwidth (MHz)	4	6	35
Type of Receiver		Logarithmic	

is to increase the transmitted energy of the laser pulse. Since the pulse length is fixed by other considerations, the peak power must be increased. This modification is easily made, since ruby lasers with peak power of up to 10^8 Watts are readily available.

2. Lidar Repetition Rate

Although the suggested repetition rate of 3 ppm is marginally adequate for the meteorological observations discussed in this report, this repetition rate does severely limit the number of observations which can be made in a short time period. Accordingly, the greatest improvement in system performance can be achieved by increasing the lidar repetition rate. The addition of a liquid-cooled ruby laser operating at repetition rates of up to 60 pulses per minute is highly desirable.

V CONCLUSIONS AND RECOMMENDATIONS

Unless the exact origin of the meteorological angels that appeared on the microwave radar scope need to be identified, it is believed that further observations of the clear lower atmosphere with 8.6 mm radar serve no useful purpose in view of the large capability of the lidar to map the structure of the clear atmosphere. Further improvements in the total power output and the receiver sensitivity would not greatly improve the present performance of the Stanford Research Institute microwave radar. On the other hand, there is little doubt about the usefulness of the microwave radar in investigating cloud structure, especially when the vertical profiles of signal intensity from the radar are combined with those obtained from the lidar in the case of stratiform clouds.

From the volume of collected data it was evident that the lidar identifies an atmospheric structure that as yet has been largely unexplored with respect to its physical significance. The major problem is to interpret the various layers of lidar echoes that were observed in the lower 2000 m of the atmosphere. A positive identification of these echoes in terms of aerosol, humidity, temperature, and thermal stability depends on the availability of measurements from instrumentation that can be launched at the local observation site. Such instrumentation should be able to measure the vertical structure of the lower atmosphere on a scale comparable to that provided by the lidar data. The Oakland radiosonde ascent is inadequate in these respects.

There was also evidence from the collected data that transient echoes of the type classified as "angels" in radar data are present in the lidar data. However, firmer evidence may have to await higher pulse-rate capabilities.

On the basis of the study presented above, the following is recommended:

(1) A continued effort should be made to quantitatively interpret lidar data of the clear atmosphere. This involves:

   (a) Calibrating, in more detail, the lidar equipment that is being used so that returned signals can be quantatized with a high degree of confidence

   (b) Making lidar observations of the clear lower atmosphere that are more continuous in time than hitherto attempted. Data collected so far show that short-period fluctuations in height are present in some of the layers detected by the lidar. Such time-dependent behavior should be further investigated. Furthermore, clear-air data that can be quantatized will enhance atmospheric models of backscattering and attenuation such as constructed by Elterman

   (c) Measuring the vertical structure of aerosol, humidity, temperature, and possibly turbulence using an instrument package attached to a tethered balloon. Without such measurements the nature of the echoes detected by the lidar are only speculative. A quantitative assessment of lidar data requires positive identification of the atmospheric properties that are measured.

(2) A ruby lidar with a high pulse rate (60 pps) is currently being developed at the Institute. When such a lidar becomes available, observations of the lower atmosphere should be made. Such observations provide much more detail than is currently obtained. They can help to define the type of lidar data that are suitable for meteorological use, and can confirm the existence of angels in lidar data.

(3) There is promise that such physical characteristics of stratus clouds as liquid-water content may be obtained by considering the difference in shape between the vertical profiles of the microwave radar and the ruby lidar for these clouds. Both actual measurements and theoretical computations are necessary for a further investigation.

BIBLIOGRAPHY

Abella, I. D., and H. Z. Cummings, "Thermal Tuning of Ruby Optical Masers," J. Appl. Phys., Vol. 32, pp. 1177-1178 (June 1961).

Air Weather Service, "Category III Test Report for AN/TPQ-11 Cloud Height Set," Headquarters, Air Weather Service, Scott Air Force Base, Illinois (September 1961).

Atlas, D., 1959, "Radar Studies of Meteorological Angel Echoes," J. Atmos. & Terres. Phys., Vol. 15, Nos. 3/4, pp. 262-287.

Atlas, D., 1960: "Possible Key to the Dilemma of Meteorological Angel Echoes," J. Meteorol., Vol. 17, No. 2, pp. 95-103.

Borovikov, A. M., et al., Chap. II of Cloud Physics, Ed. by A. Kh. Khrgian, Leningrad, USSR, 1961.

Collis, R. T. H., "Lidar: A New Atmospheric Probe," Quart. J. Roy. Meteorol. Soc., Vol. 92, No. 392 (April 1966).

Harper, W. G., "Examples of Cloud Detection with 8.6-Millimeter Radar," The Meteorol. Mag., Vol. 95, No. 1125, pp. 106-112 (1966).

Helstrom, C. W., "The Detection and Resolution of Optical Signals," IEEE Trans. on Info. Theory, Vol. IT-10, No. 4, pp. 275-287 (1964).

Katzenstein, K., and I. Marson, "A K_a-Band Radar for Cloud Base and Top Measurements," IRE International Convention Record, Part 5, pp. 105-112 (1961).

Ligda, M. G. H., "The Laser in Meteorology," Discovery (July 1965).

Long, R. K., and C. H. Boehnker, "Measured Atmospheric Absorption at Ruby Optical Maser Wavelengths," Ohio University Research Foundation, Contract AF 33(657)-11195 (June 1965).

Marshall, J. S., and W. Hitschfeld, "Interpretation of the Fluctuating Echo from Randomly Distributed Scatterers, Part I," Canad. J. Phys., Vol. 31, pp. 962-994 (1953).

Northend, C. A., R. C. Honey, and W. E. Evans, "Laser Radar (Lidar) for Meteorological Observations, "Rev. Sci. Instr., Vol. 37, No. 4, pp. 393-400 (April 1966).

Petrocchi, P. J., and W. H. Paulsen, "Meteorological Significance of Vertical Density of Clouds and Precipitation Obtained with the AN/TPQ-11 Radar," Twelfth Conference of Radar Meteorology, Norman, Oklahoma, 17-24 October 1966, pp. 467-469.

Plank, V. G., "A Meteorological Study of Radar Angels," Geophysics Research Paper No. 52, Air Force Cambridge Research Center (1956).

Sal'man, E. M., and G. B. Brylev, "The Relation Between the Thermodynamic State of the Atmosphere and Radar Echoes from a Clear Sky," Translated by AMS under Contract AF19(628)-3880 for AFCRL, Office of Aerospace Research, USSAF, L. G. Hanscom Field, Bedford, Massachusetts (November 1965).

Wilk, E. K., "Evaluation of the AN/APQ-39 (XA-3) Cloud Detector Radar," Final Report on Contract AF 19(604)-1395, Illinois State Water Survey, Meteorological Laboratory, Urbana, Illinois (1958).

Zobel, R. F., "Temperature and Humidity Changes in the Lowest Few Thousand Feet of Atmosphere," Quart. J. Roy. Meteorol. Soc., Vol. 92, No. 392, pp. 196-210 (1966).

UNCLASSIFIED

Security Classification

DOCUMENT CONTROL DATA - R&D

(Security classification of title, body of abstract and indexing annotation must be entered when the overall report is classified)

1. ORIGINATING ACTIVITY *(Corporate author)*

Stanford Research Institute
Menlo Park, California

2a. REPORT SECURITY CLASSIFICATION
UNCLASSIFIED

2b. GROUP

3. REPORT TITLE

LIDAR-RADAR LOWER ATMOSPHERIC OBSERVATIONS

4. DESCRIPTIVE NOTES *(Type of report and inclusive dates)*

Final Scientific Report Period covered: 1 April '66 thru 14 Nov. '66 Approved: 16 Jan. '67

5. AUTHOR(S) *(Last name, first name, initial)*

Viezee, William Oblanas, John

6. REPORT DATE	7a. TOTAL NO. OF PAGES	7b. NO. OF REFS
14 December 1966	64	18

8a. CONTRACT OR GRANT NO.	9a. ORIGINATOR'S REPORT NUMBER(S)
AF19(628)-5976	SRI Project 5982, Final Report
b. PROJECT AND TASK NO. 6670-07	
c. DOD ELEMENT 62405394	9b. OTHER REPORT NO(S) *(Any other numbers that may be assigned this report)* AFCRL-67-0013
d. DOD SUBELEMENT 681000	

10. AVAILABILITY/LIMITATION NOTICES

DISTRIBUTION OF THIS DOCUMENT IS UNLIMITED

11. SUPPLEMENTARY NOTES

12. SPONSORING MILITARY ACTIVITY

Hq. AFCRL, [illegible]
United States Air Force
L G Hanscom Field, Bedford, Mass. 01730

13. ABSTRACT

Simultaneous observations of the lower [illegible] with lidar (laser radar) and microwave radar are summarized. The observations are [illegible] in space to the location of Stanford Research Institute, Menlo Park, California, [illegible] time to June, August, and September 1966. Lidar echoes from the clear lower atmosphere are compared with the temperature and humidity data from the rawinsonde ascents made at Oakland, California.

During clear skies, no radar or lidar echoes were observed above 2000 m. Below this level the atmospheric structure that was analyzed from the lidar data showed a diurnal variation similar to that of the thermal stability of the atmosphere. Other time-dependent variations that were evident in the data are believed to be related to short period changes in the height of the top of the marine layer. No specific relationship was found between the lidar data and the rawinsonde data from Oakland.

Radar echoes observed in the clear lower atmosphere were classified as meteorological angels.

DD FORM 1 JAN 64 1473

UNCLASSIFIED

Security Classification

14. KEY WORDS	LINK A		LINK B		LINK C	
	ROLE	WT	ROLE	WT	ROLE	WT
Lower Atmospheric Observations						
Lidar Observations						
Microwave Radar Observations						
Meteorological Angels						
Marine Layer						
Laser Radar						

INSTRUCTIONS

1. ORIGINATING ACTIVITY: Enter the name and address of the contractor, subcontractor, grantee, Department of Defense activity or other organization *(corporate author)* issuing the report.

2a. REPORT SECURITY CLASSIFICATION: Enter the overall security classification of the report. Indicate whether "Restricted Data" is included. Marking is to be in accordance with appropriate security regulations.

2b. GROUP: Automatic downgrading is specified in DoD Directive 5200.10 and Armed Forces Industrial Manual. Enter the group number. Also, when applicable, show that optional markings have been used for Group 3 and Group 4 as authorized.

3. REPORT TITLE: Enter the complete report title in all capital letters. Titles in all cases should be unclassified. If a meaningful title cannot be selected without classification, show title classification in all capitals in parenthesis immediately following the title.

4. DESCRIPTIVE NOTES: If appropriate, enter the type of report, e.g., interim, progress, summary, annual, or final. Give the inclusive dates when a specific reporting period is covered.

5. AUTHOR(S): Enter the name(s) of author(s) as shown on or in the report. Enter last name, first name, middle initial. If military, show rank and branch of service. The name of the principal author is an absolute minimum requirement.

6. REPORT DATE: Enter the date of the report as day, month, year, or month, year. If more than one date appears on the report, use date of publication.

7a. TOTAL NUMBER OF PAGES: The total page count should follow normal pagination procedures, i.e., enter the number of pages containing information.

7b. NUMBER OF REFERENCES: Enter the total number of references cited in the report.

8a. CONTRACT OR GRANT NUMBER: If appropriate, enter the applicable number of the contract or grant under which the report was written.

8b, 8c, & 8d. PROJECT NUMBER: Enter the appropriate military department identification, such as project number, subproject number, system numbers, task number, etc.

9a. ORIGINATOR'S REPORT NUMBER(S): Enter the official report number by which the document will be identified and controlled by the originating activity. This number must be unique to this report.

9b. OTHER REPORT NUMBER(S): If the report has been assigned any other report numbers *(either by the originator or by the sponsor)*, also enter this number(s).

10. AVAILABILITY/LIMITATION NOTICES: Enter any limitations on further dissemination of the report, other than those imposed by security classification, using standard statements such as:

(1) "Qualified requesters may obtain copies of this report from DDC."

(2) "Foreign announcement and dissemination of this report by DDC is not authorized."

(3) "U. S. Government agencies may obtain copies of this report directly from DDC. Other qualified DDC users shall request through _____."

(4) "U. S. military agencies may obtain copies of this report directly from DDC. Other qualified users shall request through _____."

(5) "All distribution of this report is controlled. Qualified DDC users shall request through _____."

If the report has been furnished to the Office of Technical Services, Department of Commerce, for sale to the public, indicate this fact and enter the price, if known.

11. SUPPLEMENTARY NOTES: Use for additional explanatory notes.

12. SPONSORING MILITARY ACTIVITY: Enter the name of the departmental project office or laboratory sponsoring *(paying for)* the research and development. Include address.

13. ABSTRACT: Enter an abstract giving a brief and factual summary of the document indicative of the report, even though it may also appear elsewhere in the body of the technical report. If additional space is required, a continuation sheet shall be attached.

It is highly desirable that the abstract of classified reports be unclassified. Each paragraph of the abstract shall end with an indication of the military security classification of the information in the paragraph, represented as *(TS), (S), (C), or (U).*

There is no limitation on the length of the abstract. However, the suggested length is from 150 to 225 words.

14. KEY WORDS: Key words are technically meaningful terms or short phrases that characterize a report and may be used as index entries for cataloging the report. Key words must be selected so that no security classification is required. Identifiers, such as equipment model designation, trade name, military project code name, geographic location, may be used as key words but will be followed by an indication of technical context. The assignment of links, rules, and weights is optional.